Comparison of one-dimensional HEC-RAS with two-dimensional FESWMS model in flood inundation mapping

A Thesis

Submitted to the Faculty

of

Purdue University

by

Aaron Christopher Cook

In Partial Fulfillment of the

Requirements for the Degree

of

Master of Science in Civil Engineering

May 2008

Purdue University

West Lafayette, Indiana

To my parents, my dog, and the rest of my family.

ACKNOWLEDGMENTS

The data for this study was provided by the North Carolina Floodplain Mapping Program (NCFMP) and Fort Bend County, Texas. This study would not have been possible without this data.

I would like to thank my advisor Dr. Venkatesh Merwade for all his support and time. I would also like to thank my committee members Dr. Rao Govindaraju and Dr. Dennis Lyn.

Finally, I would like to thank my officemates Emily, Jared, Mark, Megan and Young Hun and the rest of the Hydraulic/Hydrology Group.

TABLE OF CONTENTS

Page

Page

Page

LIST OF TABLES

LIST OF FIGURES

Figure Page

Page

ABBREVIATIONS

1D	One-dimensional
2D	Two-dimensional
ASCII	American Standard Code for Information Interchange
DEM	Digital Elevation Model
DTM	Digital Terrain Model
DFIRM	Digital Flood Insurance Rate Map
FEMA	Federal Emergency Management Agency
FESWMS	Finite-Element Surface-Water Modeling System
FST2DH	Depth-Averaged Flow and Sediment Transport Model
GIS	Geographic Information System
HEC-RAS	Hydrologic Engineering Center River Analysis System
IfSAR	Interferometric Synthetic Aperture Radar
LiDAR	Light Detection and Ranging
NED	National Elevation Data
RMSE	Root Mean Squared Error
SMS	Surface-water Modeling System
SRTM	Shuttle Radar Topography Mission
USGS	United States Geological Survey

ABSTRACT

Cook, Aaron Christopher. MSCE, Purdue University, May, 2008. Comparison of one-dimensional HEC-RAS with two-dimensional FESWMS model in flood inundation mapping. Major Professor: Venkatesh Merwade.

Flood inundation mapping is influenced by many factors such as the quality of terrain data (digital elevation model, DEM), the cross-sectional configuration, and the use of a one (1D) or two-dimensional (2D) hydraulic model. The increasing availability of high resolution topographic data, development of two- and three- dimensional hydrodynamic models, and access to fast computing computers is revolutionizing the flood inundation mapping process. The objectives of this study are to compare the effect of topographic data, geometric configuration (cross-section spacing, finite element mesh resolution), and use of one and two-dimensional hydrodynamic models on the flood inundation mapping process. By using different topographic datasets (USGS DEM, surveyed cross-sections, and LiDAR) and two types of models (1D HEC-RAS and 2D FESWMS) on two study reaches (Strouds Creek in North Carolina and the Brazos River in Texas); the sensitivity of hydraulic modeling and flood inundation mapping to terrain data, geometric configuration, and model type is analyzed. HEC-GeoRAS (ArcGIS version), and Surfacewater Modeling System (SMS) are used as pre- and post-processing tools to prepare model inputs, execute models, and delineate flood inundation maps. The results from this study show that inundation extent increases as the resolution of the DEM decreases for both the one- and two-dimensional model. The higher resolution DEMs are more susceptible to changes in both cross-sectional modification and mesh resolution. The results also show that increasing the number of cross-sections in a one-dimensional simulation generally increases the inundation extent except near levees, where the results are complex, and that cross-sectional modifications alter high resolution DEMs more than

low resolution DEMs. Mesh resolution is shown to change the inundation extent less than changing either the DEM or the cross-sectional configuration and changes the inundation area by a maximum of 5% for both study areas. In general, FESWMS predicts a larger inundation extent for the higher resolution DEMs, while HEC-RAS predicts a higher or similar inundation extent for the lower resolution DEMS. Increasing the number of cross sections for the higher resolution DEMs produces inundation extent more similar to the two-dimensional model.

CHAPTER 1. INTRODUCTION

1.1. Introduction

Hydraulic modeling and flood inundation mapping are performed in order to predict important information from a flood event including the extent of inundation and water surface elevations at specific locations. A hydraulic model is essentially a representation of the processes that occur during a flood event. The processes needing to be modeled are often up for debate, as many different simplifications and assumptions have been made to create models capable of accurately representing compound channel flow while being computationally efficient. A compound channel can be described as the combination of the main river channel with floodplain areas on either side of the main channel. When the depth of flow during a flood event exceeds the height of the main channel, the flow expands into the relatively flat floodplains. In practice, high flows are often simulated using one-dimensional or two-dimensional models with a steady-state assumption. Flow processes in compound channels include momentum exchange between fast moving flow in the main channel and slower moving flow in the floodplains, formation of turbulent eddies, and formation of shear layers between the main channel flow and storage areas in the floodplain (Bates et al., 2005).

In one-dimensional hydraulic modeling, it is assumed that all water flows in the longitudinal direction. One-dimensional models represent the terrain as a sequence of cross-sections and simulate flow to estimate the average velocity and water depth at each cross-section. In two-dimensional models, water is allowed to move both in the longitudinal and lateral directions, while velocity is assumed to be negligible in the vertical direction. Unlike one-dimensional models, two-dimensional models represent the terrain as a continuous surface through a finite element mesh. Due to the continuous

representation of the terrain, two-dimensional models are able to characterize the lateral interaction of flow between the main channel and the floodplain. One-dimensional models are generally very efficient but have disadvantages including the inability to simulate the lateral diffusion of the flood wave and the representation of topography as cross-sections rather than as a surface (Hunter et al., 2007). In two-dimensional modeling, some of the physical constraints seen in a one-dimensional model can be overcome. Given that flow can be simulated in one or two-dimensions by using either a series of cross-sections or a continuous surface, the assumptions made in hydraulic modeling as well as the quality of the terrain data and the cross-sectional configuration for a one-dimensional model or mesh resolution for a two-dimensional model will have a large impact on the resulting inundation. The objectives of this thesis are to compare the effect of topographic data, geometric configuration (cross-section spacing or mesh resolution), and type of model (1D or 2D) in flood inundation mapping.

1.2. Approach

The objectives of this thesis are accomplished by comparing the results of the one-dimensional model HEC-RAS (Hydrologic Engineering Center – River Analysis System) with the two-dimensional model FESWMS (Finite Element Surface Water Modeling System) in flood inundation by using four topographic datasets and different cross-sectional configuration or mesh resolution. Both one-dimensional and two-dimensional simulations are performed on reaches of the Brazos River in Texas and Strouds Creek in North Carolina using four types of topographic datasets; Light Detection and Ranging (LiDAR), National Elevation Dataset (NED) 30 m, NED 10 m, and a custom dataset created by merging LiDAR data with surveyed cross-sections of the main channel. Typically, surface datasets such as NED or LiDAR do not include main channel bathymetry and therefore; a custom dataset is created in this study that includes cross-section data integrated with the LiDAR dataset. The geometric configurations for the one-dimensional and two-dimensional models are investigated by changing the cross-sectional configuration and the mesh resolution, respectively, for each topographic

dataset. For Strouds Creek, 18 cross-sectional configurations and 2 mesh resolutions are evaluated, while for the Brazos River, 12 cross-sectional configurations and 2 mesh resolutions are evaluated. The 100-year flow and one-dimensional model that are developed as part of the Federal Emergency Management Agency Digital Flood Insurance Rate Map (FEMA DFIRM) programs are obtained for both Strouds Creek and the Brazos River. The result from each simulation is compared to the base FEMA models to investigate the effect of topographic data, geometric configuration, and model type on flood inundation modeling. It should be noted that this thesis is not intended to calibrate models or validate results. The simulation results presented here are meant only to show the differences in modeling approaches as well as to show how changes in the digital elevation model (DEM) or resolution (mesh or cross-section) will change the extent of the floodplain.

1.3. Thesis Organization

This thesis is organized in 6 chapters. Chapter 2 presents a literature review comprised of a brief overview of the one and two-dimensional models used for this thesis, studies performed to compare 1D and 2D models, studies performed to analyze model geometry, and studies performed to analyze topography. Chapter 3 presents the study area and data. In this section, important information for both study reaches as well as the four topographic datasets is presented. Chapter 4 presents the methodology used to produce the results presented in this thesis. First, the methodology used for the one-dimensional floodplain mapping process is presented, followed by the methodology for the two-dimensional process used for Strouds Creek and the Brazos River. Chapter 5 presents the results. In the results section, the effects of topography and geometry are evaluated for the one-dimensional model for both Strouds Creek and the Brazos River. Next, the effects of topography and geometry are evaluated for the two-dimensional model for both Strouds Creek and the Brazos River. Finally, a comparison is made between the one-dimensional model and the two-dimensional model for flood inundation mapping. Chapter 6 presents a summary of the results and the conclusions.

CHAPTER 2. LITERATURE REVIEW

2.1. Introduction

In this paper, three main topics are analyzed; a comparison of one-dimensional and two-dimensional hydraulic models, effect of topographic data on the hydraulic models, and the effect of geometry on the hydraulic models. The comparison of one-dimensional and two-dimensional models, along with case studies comparing one and two-dimensional models, case studies using either a one or two-dimensional model, and case studies using a combined one-dimensional two-dimensional model is presented in Section 2.2. The effect of topographic data on the hydraulic models is presented in Section 2.3 and the effect of geometric data on the hydraulic models is presented in Section 2.4. An additional section is presented to discuss model parameters for both one- and two-dimensional models.

2.2. Comparison of 1D and 2D hydraulic models

In flood inundation modeling, a distinction must be made between one- and two-dimensional hydraulic models. One-dimensional models treat flow through both the channel and floodplain as only in the longitudinal direction. The equations for modeling one-dimensional flow are derived from the conservation of mass and conservation of momentum equations between adjacent cross-sections (Bates et al., 2005). Two-dimensional hydraulic models are based on integration over the flow depth to obtain depth averaged velocity values and are solved using an appropriate numerical approach such as a finite element model. A brief description of the one-dimensional model HEC-RAS and the two-dimensional model FEWSMS is presented in the following sections.

2.2.1. HEC-RAS

Developed by the U.S. Army Corps of Engineers, HEC-RAS allows users to perform one-dimensional steady and unsteady flow calculations (HEC, 2002). In a HEC-RAS steady state simulation, water surface profiles are computed from one cross-section to the next by solving the standard step iterative procedure to solve the energy equation. The energy equation is intended to calculate water surface profiles for steady gradually varied flow. The energy equation is shown in Equation 2.1 for two adjacent cross-sections XS1 and XS2

$$Y_2 + Z_2 + \frac{\alpha_2 V_2^2}{2g} = Y_1 + Z_1 + \frac{\alpha_1 V_1^2}{2g} + h_e \qquad \text{Equation 2.1}$$

Where Y_1 and Y_2 are depths of water at adjacent XS1 and XS2, Z_1 and Z_2 are elevations of the main channel inverts, V_1 and V_2 are average velocities (total discharge/ total flow area), α_1 and α_2 are velocity weighting coefficients, g is the gravitational acceleration, h_e is energy head loss. The energy head loss term is defined in Equation 2.2.

$$h_e = L\bar{S}_f + C\left|\frac{\alpha_2 V_2^2}{2g} - \frac{\alpha_1 V_1^2}{2g}\right| \qquad \text{Equation 2.2}$$

Where L is discharge weighted reach length, $\bar{S}_f$ is representative friction slope between XS1 and XS2, and C is an expansion or contraction loss coefficient. The representative friction slope using the average conveyance equation and the distance weighted reach length are defined in Equation 2.3 and Equation 2.4, respectively.

$$\bar{S}_f = \left(\frac{Q_1 + Q_2}{K_1 + K_2}\right)^2 \qquad \text{Equation 2.3}$$

$$L = \frac{L_{lob}\overline{Q}_{lob} + L_{ch}\overline{Q}_{ch} + L_{rob}\overline{Q}_{rob}}{\overline{Q}_{lob} + \overline{Q}_{ch} + \overline{Q}_{rob}}$$ Equation 2.4

Where K is conveyance, L_{lob}, L_{ch}, and L_{rob} are cross-section reach lengths for flow in the left over-bank, main channel, and right over-bank, respectively, and $\overline{Q}_{lob}$, $\overline{Q}_{ch}$, and $\overline{Q}_{rob}$ are arithmetic average of the flows between sections for the left over-bank, main channel, and right over-bank, respectively.

To determine total conveyance and the velocity coefficient for a cross-section, HEC-RAS subdivides flow in the main channel from the over-banks. Conveyance is calculated for each subdivision using Equation 2.5 and Equation 2.6.

$$Q = KS_f^{1/2}$$ Equation 2.5

$$K = \frac{1.486}{n}AR^{2/3}$$ Equation 2.6

Where K is conveyance for the subdivision, n is Manning's roughness coefficient for the subdivision, A is flow area for the subdivision, and R is hydraulic radius for each subdivision. The total conveyance for each subdivision is calculated as the sum of the conveyance from the left over-bank, main channel, and right over-bank. Flow in the main channel is subdivided only when the Manning's roughness coefficient changes within the channel area. The composite main channel Manning's roughness coefficient is defined in Equation 2.7.

$$n_c = \left[\frac{\sum_{i=1}^{N} \left(P_i n_i^{1.5} \right)}{P} \right]^{2/3}$$

Equation 2.7

Where n_c is the composite or equivalent coefficient of roughness, P is the wetted perimeter of the entire main channel, P_i is the wetted perimeter of subdivision i, and n_i is the coefficient of roughness for subdivision i.

Limitations in the HEC-RAS steady flow simulation include the assumptions that the flow is steady, the flow is gradually varied, the flow is one-dimensional, and the river channels have small slopes.

For situations when the flow may be rapidly varied, the momentum equation is used to solve the water surface profiles. These situations include hydraulics of bridges, river confluences, and mixed flow regimes such as hydraulic jumps. The momentum equation used in HEC-RAS is shown in Equation 2.8.

$$\frac{Q_2 \beta_2}{g A_2} + A_2 \overline{Y}_2 + \left(\frac{A_1 + A_2}{2} \right) L S_0 - \left(\frac{A_1 + A_2}{2} \right) L \overline{S}_f = \frac{Q_1 \beta_1}{g A_1} + A_1 \overline{Y}_1$$

Equation 2.8

Where β is momentum coefficient that accounts for a varying velocity distribution in irregular channels, $\overline{Y}_1$ and $\overline{Y}_2$ are depths measured from the water surface to the centroid of the cross-sectional area at XS1 and XS2, Q_1 and Q_2 are discharge at locations XS1 and XS2, A_1 and A_2 are wetted area of the cross-section at locations XS1 and XS2, L is distance between sections XS1 and XS2 along the channel, S_0 is slope of the channel based on mean bed elevations, and $\overline{S}_f$ is slope of the energy grade line. Additional information can be found in the HEC-RAS Hydraulic Reference Manual (HEC, 2002).

Required model parameters for HEC-RAS include topographic data in the form of a series of cross-sections, a friction parameter in the form of Manning's n values across each cross-section, and flow data including flow rates, flow change locations, and boundary conditions. For a steady state sub-critical simulation, the boundary condition is a known downstream water surface elevation.

2.2.2. FESWMS

The depth-averaged Flow and Sediment Transport Model (FST2DH), part of the Federal Highway Administration's FESWMS, is a computer program that simulates movement of water and non-cohesive sediment in rivers, estuaries, and coastal waters. FST2DH applies the finite element method to solve steady or unsteady flow equations that describe the two-dimensional depth averaged surface water flow (FESWMS, 2002). FST2DH is used when vertical velocities are assumed to be negligible compared to lateral flow.

The finite element method is a numerical procedure for solving differential equations. In this approach, continuous quantities are approximated by sets of variables at discrete locations forming a network (mesh). FST2DH uses the Galerkin finite element method to solve the governing differential equations discussed in the following paragraph.

The Galerkin finite element method begins by dividing a physical region into triangular or quadrilateral elements. These elements are defined by nodes and vertices along their boundary. Dependent variables are approximated within each element using values previously defined at the node points of an element along with sets of interpolation functions. In FST2DH, a mixed interpolation function is used in which quadratic functions are used to interpolate unit flow rates at all nodes of an element and linear interpolation is used to interpolate water depth at the vertices of an element. The mixed interpolation function is used to stabilize the numerical solution. The method of weighted residuals, a mathematical technique used for approximating solutions to partial

differential equations in which residuals to the solution are made to sum to zero, is applied to the governing differential equations. More information on the Galerkin finite element method and the method of weighted residuals can be found in the FESWMS (2002).

The two-dimensional depth averaged flow equations used in FST2DH are described in this section. Depth-averaged velocities in the horizontal x and y coordinate directions are defined in Equation 2.9 and Equation 2.10, respectively.

$$U = \frac{1}{H}\int_{z_b}^{z_w} u\, dz \qquad \text{Equation 2.9}$$

$$V = \frac{1}{H}\int_{z_b}^{z_w} \mathrm{v}\, dz \qquad \text{Equation 2.10}$$

Where H is water depth, z is vertical direction, z_b is bed elevation, z_w is water surface elevation, U is horizontal velocity in the x-direction at a point along the vertical coordinate, V is horizontal velocity in the y-direction at a point along the vertical coordinate.

Equations describing the depth-averaged surface water flow are found by integrating the three-dimensional mass and momentum transport equations with respect to the vertical coordinates from the bed to the water surface. In this approach, vertical velocities and accelerations are assumed to be negligible. The vertically-integrated continuity equation is shown in Equation 2.11.

$$\frac{\partial z_w}{\partial t} + \frac{\partial q_1}{\partial x} + \frac{\partial q_2}{\partial y} = q_m \qquad \text{Equation 2.11}$$

Where $q_1 = UH$ is unit flow rate in the x direction, $q_2 = VH$ is unit flow rate in the y direction, q_m is mass inflow rate or outflow rate per unit area. Water mass density is considered constant throughout the modeled region.

Equations describing momentum transport in the x and y directions are shown in Equation 2.12 and Equation 2.13.

$$\frac{\partial q_1}{\partial t} + \frac{\partial}{\partial x}\left(\beta \frac{q_1^2}{H} + \frac{1}{2} g H^2\right) + \frac{\partial}{\partial y}\left(\beta \frac{q_1 q_2}{H}\right) + gH \frac{\partial z_b}{\partial x} + \frac{H}{\rho}\frac{\partial p_a}{\partial x} - \Omega q_2 + \frac{1}{\rho}\left[\tau_{bx} - \tau_{sx} - \frac{\partial(H\tau_{xx})}{\partial x} - \frac{\partial(H\tau_{xy})}{\partial y}\right] = 0 \quad \text{Equation 2.12}$$

$$\frac{\partial q_2}{\partial t} + \frac{\partial}{\partial y}\left(\beta \frac{q_1^2}{H} + \frac{1}{2} g H^2\right) + \frac{\partial}{\partial x}\left(\beta \frac{q_1 q_2}{H}\right) + gH \frac{\partial z_b}{\partial y} + \frac{H}{\rho}\frac{\partial p_a}{\partial y} - \Omega q_1 + + \frac{1}{\rho}\left[\tau_{by} - \tau_{sy} - \frac{\partial(H\tau_{yx})}{\partial x} - \frac{\partial(H\tau_{yy})}{\partial y}\right] = 0 \quad \text{Equation 2.13}$$

Where β is isotropic momentum flux coefficient that accounts for the variation of velocity in the vertical direction, ρ is water mass density, p_a is atmospheric pressure at the surface, Ω is the Coriolis parameter, τ_{sx} and τ_{sy} are surface shear stresses acting in the x and y directions, respectively, and τ_{xx}, τ_{xy}, and τ_{yy} are shear stresses caused by turbulence. More information regarding the governing equations used by FST2DH can be found in the FESWMS (2002).

Required model parameters for FESWMS include topographic data in the form of a continuous surface represented by a finite element mesh, a friction parameter for each element in the form of a Manning's n value, flow data, and a turbulent parameter. The steady flow sub-critical simulation in FESWMS requires an upstream flow rate and a downstream known water surface elevation. The only turbulent parameter in FESWMS is the eddy viscosity. The eddy viscosity is further discussed in Section 2.5.

2.2.3. Case studies using 1D hydraulic models

Case studies have been performed using one-dimensional models to show the capabilities of the model being used. Some of these case studies have been performed to calibrate hydraulic models or validate results; but the main focus of these studies has been to analyze the effect of topographic data on the hydraulic model. The effect of topographic data on both one-dimensional and two-dimensional models will be further discussed in Section 2.3. This section presents results from one-dimensional case studies.

Case studies using one-dimensional models such as HEC-RAS (Brandt, 2005; Omer, 2003; and Casas, 2006), HEC-2 (Mohammed, 2006), and HEC-6 (Sinnakaudan, 2002) have been performed. In each of these studies, the goal has been to show how the effect of changes in topography will impact the floodplain. A one-dimensional model is often selected for this process because it represents the most basic approach to floodplain modeling. In each of the three studies listed above, the one-dimensional model used was successful in showing how a change in topography would affect the model. In the case study of the Linggi River in Seremban Town, Malaysia, HEC-2 was used to calibrate and validate the results. It was shown that the absolute error in predicted water surface levels was within 5% of the observed levels (Mohammed, 2006).

2.2.4. Case studies using 2D hydraulic models

Case studies have been performed using two-dimensional models to show the capabilities of the model being used. Some of these case studies have been performed to calibrate hydraulic models or validate results while some have been performed to develop flood maps of flood levels. This section presents discussion related to two-dimensional models.

A study of a 4.6 mile reach of the Flint River at Albany, Georgia was performed using FESWMS to develop incremental 1-ft flood surfaces corresponding to stream gages data. In this study, the model was calibrated using a 120,000 cfs flow by adjusting the eddy

viscosity until the water surface elevation determined by the model matched the stream gage (Musser and Dyer, 2005). Results show that the model was able to be validated against a flow of 86,000 cfs.

In a similar study performed by the United States Geological Survey (USGS) on the Ohio River, Jefferson County, Kentucky, calibration and validation of the two-dimensional Resource Management Associates-2 (RMA-2) were explored (Wagner and Mueller, 2001). The model was calibrated at a low flow value (35,000 cfs) and validated with data at a high flow (390,000 cfs). From the calibration and validation, it was determined that the RMA-2 model was a good representation of the Ohio River below steady flow discharges of approximately 400,000 cfs.

In another study designed to evaluate the capabilities of two-dimensional models on the Lower Blue River in Kansas City, Missouri, FESWMS was selected to perform steady-state flood flows for a hydraulically complex region of the river to determine the estimated extent of flood inundation (Kelly and Rydlund, 2005). The FESWMS simulations provided information as to the needed design of hydraulic structures and produced flood inundation maps at 2-ft water level intervals. According to this study, the flood inundation maps created represent a substantial increase in the capability of public officials and residents to minimize flood deaths and damage in the flood plain of the Lower Blue River.

2.2.5. Case studies comparing 1D and 2D hydraulic models

Recent research has been conducted on comparing one-dimensional models with two-dimensional models, including using HEC-RAS, LISFLOOD-FP, a raster based model, and TELEMAC-2D, a finite element model, on a 60 kilometer reach of the river Severn, UK (Horritt and Bates, 2002). LISFLOOD-FP is a combined 1D-2D model solving 1D continuity and momentum equations in the main channel and 2D continuity and momentum equations in the floodplain and TELEMAC-2D solves the 2D shallow water

equations. In this study, it was shown that HEC-RAS and TELEMAC-2D are both capable of being calibrated against discharge or inundated area while LISFLOOD-FP must be calibrated against an independent inundated area to produce acceptable results.

Similarly, a study performed on a 25 kilometer reach of the Consumnes River in the Sacramento Valley, California compared three models; Water-Surface PROfile Computations (WSPRO), MIKE 11, and MIKE 21 on a 30 meter resolution DEM (Juza and Barad, 2000). WSPRO is a 1D model similar to HEC-RAS, MIKE 11 is an unsteady-looped 1D model based on the Saint-Venant equations, and MIKE 21 is a 2D implicit finite difference scheme used for unsteady flows. The results show that there are significant differences in water surface elevations between WSPRO and MIKE 11 due to the fact that MIKE 11 can characterize exchanges between the floodplain and channels, whereas WSPRO cannot. Results also indicate that the 2D model more accurately represents flow in the floodplain due to both lateral and longitudinal movement of water.

In a similar study to compare one-dimensional models with two-dimensional models, a study of the River Alzette north of Luxembourg City examined a HEC-RAS simulation with a Regression and Elevation-based Flood Information eXtraction (REFIX) simulation for a 2 meter resolution LiDAR DEM. Results indicate that the floodplain from the HEC-RAS simulation was larger than from the REFIX simulation (Schumann et al., 2007). Other studies have also shown similar results between one-dimensional and two-dimensional models such as a case study of the 1983 Rudd Creek Mudflow in Utah where water surface profiles were found to be similar between the one-dimensional HEC-2 and the two-dimensional FLO-2D (O'Brien et al., 1993).

Similarly, a study of a 6 kilometer reach of the River Wharf, UK compared inundation extent from HEC-RAS with a two-dimensional diffusion wave model (Tayefi et al., 2007). The DEM for this study was created using a combination of 58 GPS surveyed cross-sections for the main channel and remotely sensed LiDAR for the floodplains. The results from this study show that, in qualitative terms, the two-dimensional model

produces the best results although the one-dimensional model could be calibrated to produce accurate results.

Because of the increasing availability and popularity of two-dimensional flood inundation models, studies have been performed to compare the performance of multiple 2D models. In a study of three 2D models it was determined that use of a simplified 2D model would give errors of approximately 10% while offering savings in computational effort (Leopardi et al., 2002). The three models used in this case study were a complete two-dimensional model, FIVFLOOD, and two simplified models, PA-31 and MCEP.

2.2.6. Combined 1D-2D hydraulic models

A recent trend in flood inundation modeling is the use of a combined one-dimensional main channel model with a two-dimensional floodplain model. On a study of the Ticha Orlice River confluence with the Trebovka River in the Central Czech Republic, a one-dimensional floodplain model was compared with a hybrid one-dimensional two-dimensional model. In this urban setting, it was found that the results of the Sobek 1D and Sobek 1D-2D model were comparable, primarily as a result of the flood extent being constrained by road and railway embankments (Werner et al., 2005). The DEM used in this study was derived from LiDAR.

The use of a combined 1D-2D model was also used in a case study of the lower Mekong River in Thailand (Dutta et al., 2007). The model consisted of the 1D unsteady dynamic wave form of Saint Venant's equation for river channel simulation combined with 2D unsteady equations for floodplain flow. For this study, a 1 kilometer grid resolution was used due to the large basin being considered. Results indicate that this model demonstrated similar alignment with the observed data in terms of water level and discharge as well as flood extent. It was inferred that this model is a reasonable approach to predict both the magnitude and duration of flood events to a reasonable degree of accuracy. Other studies have also shown that a combined 1D-2D model produce

acceptable results in flood inundation modeling (McMillan and Brasington, 2007; Tayefi et al., 2007).

2.3. Effects of topography on hydraulic models

Due to the recent availability of high resolution elevation data such as LiDAR, it is becoming possible to develop increasingly accurate floodplain maps. In some areas in the United States as well as around the world, LiDAR elevation data, or similar resolution elevation data, are available. From recent studies, it has been proven that topography is one of the most important parameters in flood inundation modeling (Shuman et al., 2007; Haile and Reintjes, 2005) This leads to the question of how much accuracy is gained in floodplain mapping by using a higher resolution elevation dataset. The following section describes some recent studies on the effect of topography on hydraulic models.

In a recent study of the Santa Clara River near the Castaic Junction in Southern California, selected because of the availability of IfSAR (interferometric synthetic aperture radar), NED and SRTM (shuttle radar topography mission) elevation data, it was determined that the floodplain varies by at most 25%, with the NED 10 m dataset predicting the smallest area and the SRTM-3 s dataset producing the largest area (Sanders, 2007). The horizontal resolution of NED 10 m is approximately 10 meters, while the horizontal resolution of SRTM-3 s is approximately 90 meters. In the same study, an 8 kilometer reach of Buffalo Bayou near Houston, Texas was selected to validate the results. This area is characterized by a relatively flat floodplain. Available elevation datasets for this region were NED 3 m (LiDAR), NED 10 m, and NED 30 m. For the 100-year storm event, floodplain area varied by only 5% and floodplain depth varied by only 4% between the three NED terrains. Predictions for floodplain analysis were performed using the two-dimensional BreZo model.

In a similar study performed on a 2 kilometer reach of the Ter River near Sant Julia de Ramis, 5 kilometers downstream of Girona, Spain, seven digital terrain models (DTMs)

from three different sources were compared for flood inundation mapping using HEC-RAS. The three sources for the DTMs were GPS survey including bathymetry, LiDAR, and vectorial cartography from 5 meter contours. The results showed that flood inundation area increased with decreasing DEM resolution (Casas et al., 2007).

In another study to further evaluate the impact of topography on hydraulic models, a study, performed on a flood prone area drained by the Alzette River north of Luxembourg City, involved the comparison of water stages derived from LiDAR, SRTM, and topographic contours (Schumann et al., 2007). This study used the REFIX hydraulic model to determine water stages. Results from this study indicate that the root mean squared error (RMSE) of water surface elevations from LiDAR (2 meter spatial resolution) was 0.35 meters, from the topographic contours was 0.7 meters, and from SRTM (6 meter vertical precision) was 1.07 meters. The floodplain extent for the three DEMs was then compared to a HEC-RAS simulation with LiDAR derived floodplains and the Advanced Synthetic Aperture Radar (ASAR) observed flooded area. The comparisons showed that the LiDAR derived flood maps agree 75% with the observed flood, 73% with HEC-RAS, 62% with topographic contours, and 59% with SRTM.

The effect of topographic data is also examined in a study comparing the extent of flood inundation on the River Nene, Northamptonshire, UK, using three remotely sensed elevation datasets: LiDAR, stereo photogrammetry, and repeat-pass ERS interferometric SAR (InSAR) (Wilson and Atkinson, 2003). Using the LISFLOOD-FP flood inundation model, described in detail by Bates and De Roo (2000), the most accurate predictions were obtained using the LiDAR data followed by the photogrammetric data when compared to aerial photography.

2.3.1. DEM Resolution

The effects of re-sampling a DEM have also been studied. In an urban case study of the city of Tegucigalpa, Honduras, a LiDAR derived DEM was re-sampled to a resolution of

15 meters for flood inundation modeling using the combined 1D and 2D SOBEK model (Haile and Rientjes, 2005). It was found that the lowest resolution DEMs (12.5 and 15 meter) produced the largest inundation area, while the 7.5 meter DEM produced the smallest inundation area.

A similar study to evaluate the influence of re-sampling a DEM was performed on a 60 km reach of the River Severn, UK (Horrit and Bates, 2001). This study shows the effects of grid size on the raster-based flow model, LISFLOOD-FP. In this study, a 10 meter DEM was re-sampled by local averaging to scales up to 1000 meters. It was discovered that maximum performance, when compared to RADARSAT remote sensing satellite, occurred at a resolution of 100 meters, after which no improvement is seen with increasing resolution. Another study using the same approach of re-sampling a DEM to a lesser resolution was performed on the Eskilstuna River in Sweden (Brandt, 2005). From this study, it was determined that high resolution datasets lead to better inundation results than do low resolution datasets. The DEM resolution in this study ranged from 1 meter to 100 meters.

Using a similar process of re-sampling topographic data, recent studies have focused on re-sampling high resolution topographic data to receive only necessary elevation data. In a study performed on Lith Creek northwest of Laurinburg, North Carolina, vertices of a TIN derived from LiDAR were eliminated if the angular difference between adjacent normals is within the user specified tolerance (Omer et al., 2003). This technique is designed to remove redundant data and make hydrologic and hydraulic modeling more efficient. It was found that filtering the LiDAR DEM up to 4 degrees produced only a 0.5% error in inundation area while processing time savings ranged from 38% to 59%. Another study designed to use only necessary elevation data, conducted on a 12 kilometer reach of the River Stour in Dorset, UK, deals with filtering LiDAR data to include only topographically optimum data for floodplain modeling using the TELEMAC-2D model developed by Bates and Hervouet (1999). When the topographically optimum data is used to create a mesh, it is found to better represent the raw earth better than when an

elevation dataset is applied to a mesh created independent of topography and the differences are hydraulically significant (Bates et al., 2003).

2.3.2. DEM Accuracy

Other recent studies have focused on the accuracy of the DEM, not the accuracy of the floodplain. These studies are performed to show the differences and errors in certain DEMs, but are not applied to any hydraulic models. In a study of the Swift and Red Bud Creek watersheds in North Carolina, DEMs were created from LiDAR, IfSAR, NED 10 m, and NED 30 m data to test the accuracy of the methods (Hodgson et al., 2003). The root mean squared error (RMSE) for the LiDAR dataset was 93 cm, the lowest value of the four DEMs tested. The RMSE for the NED-1/3 s DEM was 163 cm, for the NED-1 s DEM was 743 cm, and for the IfSAR was 1067 cm. LiDAR and IfSAR data were collected during leaf-on conditions meaning the vegetation could have a large impact on the DEM. In a separate study of a LiDAR dataset obtained for a reach of the River Coquet, Northumberlank, UK, it was shown that deep water and vegetation introduce anomalies in the LiDAR generated surface when compared to surveyed points (Charlton et al., 2003). It was determined that LiDAR generated cross-sections are incomplete where there is deep water present and distorted where trees are present. This study specifically examined river environments, and not the elevation of the floodplain.

2.4. Effects of geometry on hydraulic models

Hydraulic model geometry, cross-section for one-dimensional models and mesh resolution for two-dimensional models, is also an important factor in floodplain mapping. The following sections describe some recent studies detailing to effect of geometry on hydraulic models. The effect of cross-sectional configuration on one-dimensional hydraulic models is presented in Section 2.4.1 and the effect of mesh configuration on two-dimensional models is presented in Section 2.4.2.

2.4.1. Effect of 1D geometry on hydraulic models

Cross-sectional resolution for one-dimensional hydraulic models is discussed in this section. According to the HEC-RAS manual, every effort should be made to obtain cross-sections that accurately represent the stream and floodplain geometry. Cross-sections are required at a representative locations throughout a stream such as where changes occur related to discharge, slope, shape, or roughness. Cross-sections are also required before and after bridges or control structures. The HEC-RAS manual also states that cross-sections spacing is a function of stream size, slope, and uniformity of the channel. This means that large uniform rivers with a flat slope will require the least number of cross-sections. According to another study, cross-sections should be surveyed at sufficiently frequent locations to describe the hydraulic behavior of the channel with acceptable precision but should be cost effective (Samuels, 1990). According to this paper, cross-sections should be placed at model limits, either side of hydraulic structures, sites of importance to the client, and at all flow or water surface elevation measurements. Other guidelines for cross-section spacing are as follows in Equation 2.14 through Equation 2.17.

$$\text{Spacing} \approx 20B \qquad \text{Equation 2.14}$$

$$\text{Maximum Spacing} = \frac{0.2D}{s} \qquad \text{Equation 2.15}$$

$$\text{Maximum Spacing} = \frac{L}{30} \qquad \text{Equation 2.16}$$

$$\text{Minimum Spacing} = \frac{10^{d-q}}{\varepsilon_s s} \qquad \text{Equation 2.17}$$

Where B is the width of the water surface, D is the bank full depth, s is main channel slope, L is the length scale of the physically important flood wave, q is the number of decimal digits of precision, d is the digits of precision lost, and ε_s is the relative error on

the surface slope. The first equation is designed as a first estimate of cross-section spacing. The cross-section spacing guidelines from this paper were designed for main channel flow only. It is expected that linking the floodplains to the main channel will result in different conclusions for cross-section spacing. Results from a one-dimensional analysis of the Pari River in Malaysia suggest that more cross-sections at lesser intervals will result in improved flood inundation (Sinnakaudan et al., 2002).

2.4.2. Effect of 2D geometry on hydraulic models

Mesh resolution has also been a topic that has been studied recently in two-dimensional hydraulic models. In a study of a purely hypothetical example river with the hydraulic model TELEMAC-2D, it was discovered that the effects of mesh resolution were at least as important as typical calibration parameters and that model response to changes in mesh resolution were highly complex (Hardy et al., 1998). It was also shown that as the resolution of the mesh increases, the extent of inundation decreases. Increasing inundation extent as a result of reduced resolution is a direct consequence of loss of topographic information in the main channel.

To further show the effect of mesh resolution on a two dimensional model, a seven kilometer reach of the River Thames, UK, was examined using a 2D finite volume model. Results from this study show that the model shows greater sensitivity to mesh resolution than to topographic sampling (Horritt et al., 2006). The sensitivity in mesh resolution was determined to be caused by larger elements not being able to represent some hydraulic features which occur at scales smaller than the element size and changes in the representation of the domain boundary due to differing element sizes.

In some recent studies using two-dimensional models, the effect of decomposing the mesh according to vegetation heights has been examined. Using LiDAR elevation data, it is possible to separate ground hits from surface object hits. Ground hits are used to construct a DEM and surface object hits are used to determine the heights of vegetation

or buildings (Mason et al., 2003). Vegetation height is then used as a friction parameter and applied to each node in a two-dimensional mesh. The detailed process of the so-called LiDAR segmentation can be found in Mason et al. (2003) and Cobby et al., (2003). This technique, combined with steady state TELEMAC-2D finite element model, was tested on a reach of the River Severn, UK, for a 50 year flood event which occurred in 1998. The results from this study show that the variable friction factor approach produced a flood extent that agreed in most places with the observed data without calibration, although the constant floodplain friction model also produced accurate results (Mason et al., 2003). Another study, performed on the same study area, found improvements in this procedure by decomposing the mesh to reflect floodplain vegetation features having differing frictional properties from their surroundings (Cobby et al., 2003). The simulated hydraulics using this approach gave a better representation of the observed flood extent than the simpler approach of sampling vegetation friction factors onto a mesh created independent of vegetation.

Other studies of mesh resolution have been performed to determine river pattern flows at smaller scales. In a study of a 400 meter reach of the North Fork of the Feather River near Belden, California, it was determined that reducing the element sizes in the vicinity of obstructions and banks is crucial to modeling flow patterns created by topographic features (Crowder and Diplas, 2000). This study was performed to determine the types of topographic features which should be included in 2D model studies and to what extent topographic features such as boulders can influence predicted flow conditions. Individual obstructions were seen to influence flow patterns up to a distance of 6-8 times the obstruction diameter.

2.5. Model Parameters

In one-dimensional models, the roughness parameter, Manning's n value, is important to the solution of the computed water surface profile, and can be use as a calibrating parameter. The equations used by HEC-RAS to determine Manning's n values are

discussed in Section 2.2.1. According to HEC (2002), the selection of an appropriate value for Manning's n is very significant to the accuracy of the computed water surface profiles. The value of Manning's n depends on a number of factors including surface roughness, vegetation, channel irregularities, size and shape of the channel, seasonal changes, temperature, and suspended material. From HEC (2002), the main channel Manning's n should be between 0.025 for a clean straight channel to 0.15 for very weedy reaches with deep pools and heavy stands of timber or brush. The Manning's n in the floodplain should be between 0.025 and 0.20. Values of Manning's n that have been used in recent studies using one-dimensional models include between 0.026 and 0.065 in the floodplains (Casas et al., 2006) and between 0.03 and 0.05 in the main channel and between 0.06 and 0.10 in the floodplains (Horritt and Bates, 2002).

In two-dimensional hydraulic models, such as FESWMS, the eddy viscosity is used as a representation of the turbulence parameters. According to FESWMS (2002), the eddy viscosity in natural channels is related to the bed shear velocity and the depth of flow by Equation 2.18.

$$V_t = (0.6 \pm 0.3) u_* H \qquad \text{Equation 2.18}$$

Where V_t is eddy viscosity, u_* is bed shear velocity, and H is depth.

The bed shear velocity can be related to the depth and slope of the channel by Equation 2.19 for uniform flow.

$$U_* = \sqrt{gHS} \qquad \text{Equation 2.19}$$

Where g is the gravitational constant and S is slope of the channel.

Also according to FESWMS (2002), the eddy viscosity coefficient usually affects the solution much less than the roughness coefficient, although the eddy viscosity can be used as a convergence parameter. Large values of eddy viscosity tend to enhance model convergence. For uniform flow, larger values of eddy viscosity only affect the water surface elevations near the downstream end of the channel. For locations where the flow is constricted, the eddy viscosity will have a large impact on the upstream water surface elevation.

Some typical values of eddy viscosity have been used in previous studies and are presented in this section. According to Zanichelli, et al., (2004), for deep channels, eddy viscosities between 2.4 and 14.4 m/s^2 are acceptable. An eddy viscosity of14.4 m^2/s corresponds to an eddy viscosity of nearly 150 ft^2/s in English units. Also according to this paper, eddy viscosity depends on element size, current speed, and the dynamic nature of the problem. Other studies have used eddy viscosities of 10 ft/s^2 for flow under bridges (Winters, 2000) and of 0.6 m^2/s for shallow water flow (Papanicolaou and Elhakeem, 2006).

The roughness parameter, Manning's n value is also an important parameter that can be used in calibrating the two-dimensional model. According to FESWMS (2002), even comparatively small changes in Manning's n can produce significant changes in the water surface profile with larger values of Manning's n producing higher water surface elevations. According to Hardy et al., (1999), the floodplain friction value has a far greater effect on the model when compared with channel friction. Values of Manning's n that have been used in recent studies include 0.025 for the main channel and between 0.056 and 0.111 in the floodplain (Hardy, et al.), between 0.02 and 0.04 in the main channel and between 0.2 and 0.1 in the floodplain (Horritt and Bates, 2002), and between 0.045 and 0.065 in the main channel (Tayefi, et al., 2007).

2.6. Summary

In this chapter, comparison of one- and two-dimensional models have been made, the effect of both topographic and geometric data on the model has been examined, and a description of important model parameters has been presented. Much of the research that has been presented in this section deals with floodplain mapping in Europe. In Europe, many hydraulic modeling and flood inundation studies have been performed including using high resolution topographic data, using two-dimensional models, and comparing one- and two-dimensional models. In the United States, most of the hydraulic modeling and flood inundation mapping is the responsibility of the FEMA DFIRM program. The FEMA DFIRM uses a one-dimensional model to develop 100-year floodplain boundaries for many areas in the United States. Case studies for specific rivers have also been performed by the USGS using two-dimensional hydrodynamic models. In most studies, only the results of the hydraulic modeling and flood inundation mapping procedure for one river have been presented. This thesis adds to current research by presenting a comparison between one- and two-dimensional models for two study areas in the United States. The effect of model geometry and topography is also presented for both study areas.

CHAPTER 3. STUDY AREA AND DATA

3.1. Introduction

This section gives an overview of the two study areas, Strouds Creek in North Carolina and the Brazos River in Texas and the data that will be used to simulate the floodplain using one- and two-dimensional hydrodynamic models. The four topographic datasets used are LiDAR, NED 10 m, NED 30 m, and an integrated DEM. Presented in the following sections are river geometry characteristics, cross section and bridge data, land use classifications in terms of the Manning's n value, and flow data at various river stations. For Strouds Creek, data is provided by the North Carolina Floodplain Mapping Program (NCFMP) while for the Brazos River, data is provided by Fort Bend County.

3.2. Description of Strouds Creek

Strouds Creek is a 4 mile long tributary of the Eno River in Orange County, North Carolina. Strouds Creek has an average width of 30 feet, an average slope of 0.56%, and is characterized by a relatively narrow floodplain with a v-shaped valley. The land use description for the Strouds Creek main channel range from a Manning's n value of 0.04 to 0.05. In the floodplains, the Manning's n value ranges from a value of 0.1 to 0.2. Figure 3.1 shows the location of Strouds Creek as well as the original cross-sectional configuration with some cross sections labeled for reference.

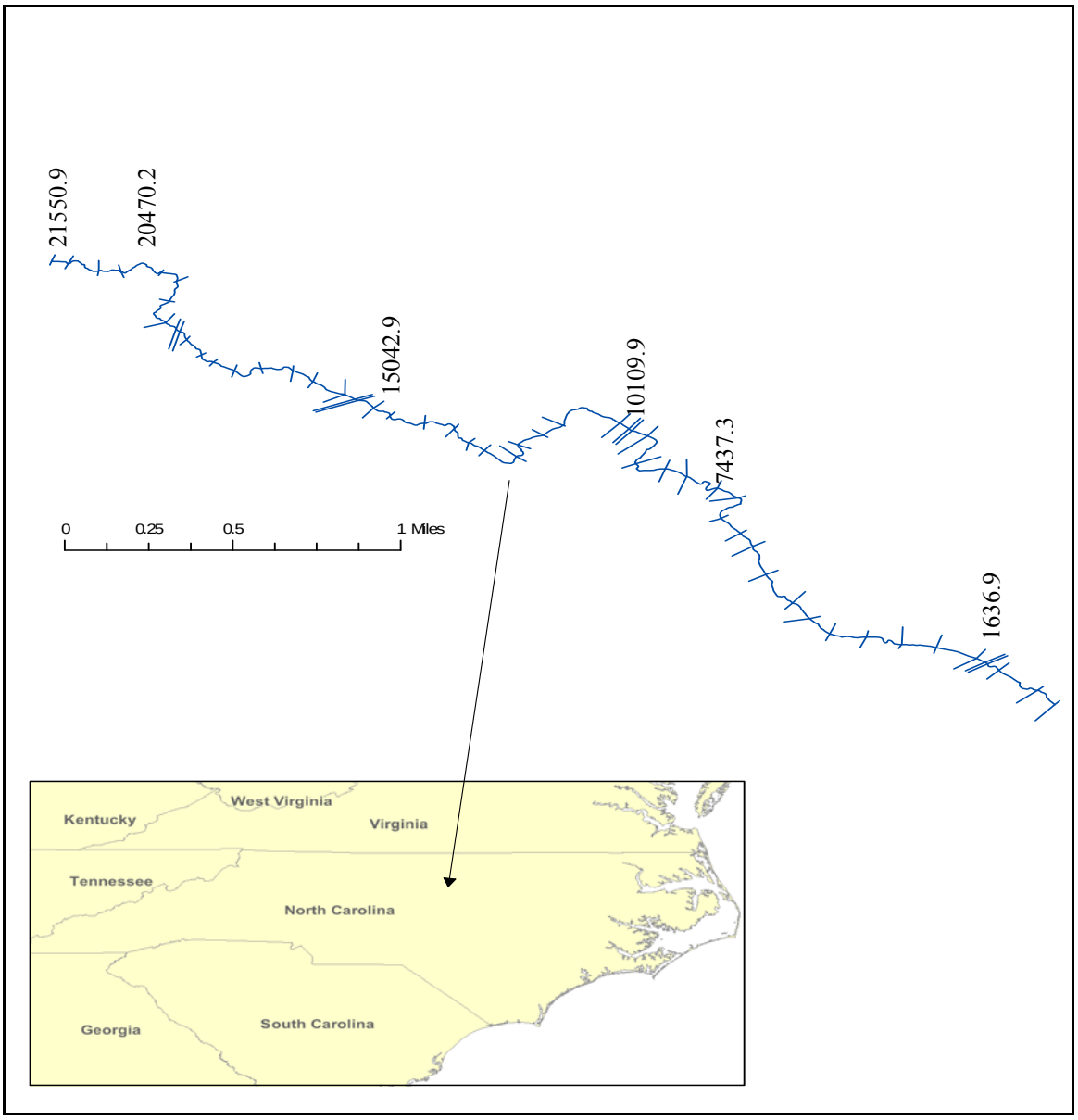

Figure 3.1 Strouds Creek Study Area

3.2.1. Cross-section and Bridge Data

The original HEC-RAS project file for Strouds Creek is obtained from the NCFMP and consists of data for 55 cross-sections, one culvert, and three bridges. The original cross-sectional configuration is shown in Figure 3.1. The original 55 cross-sections have an average width of 404 feet and average spacing between cross-sections is 396 feet.

The following section provides the characteristics of each of the three bridges and one culvert located on the reach of Strouds Creek being evaluated. For all bridges, a drag coefficient, C_d is given as 2.0 and pier shape, K as 1.25. A drag coefficient equal to 2.0 corresponds to square nose piers. A pier shape coefficient of K equal to 1.25 corresponds to a square nose and tail.

HWY 57 Culvert – Located at station 18165.6 feet.
The HWY 57 culvert road is 45 feet long. The culvert is a combination of two box shaped culverts with a span of 10 feet and a rise of 8 feet. The entrance loss coefficient and exit loss coefficient are assumed to be 0.4 and 1.0, respectively.

Governor Road Bridge – Located at station 15021.4 feet
The Governor Burke Road Bridge is 23 feet wide and 30 feet long. The bridge has no piers.

Miller Road Bridge – Located at station 9919.1 feet
The Miller Road Bridge is 30 feet wide and 80 feet long. The bridge consists of two piers, each one foot wide.

St. Mary's Road Bridge – Located at station 1475.3 feet
The St. Mary's Road Bridge is 26 feet wide and 50 feet long. The bridge consists of one pier four feet wide.

3.2.2. Flow Data

The flow data for the 100-year return period are obtained from the HEC-RAS project provided by NCFMP. Table 3.1 presents the steady state flow rates assigned at various river stations.

Table 3.1 Flow Rates for Strouds Creek

Station (ft)	Flow Rate (cfs)
21,550.9	1,427
20,470.2	1,759
15,042.9	2,288
10,109.9	2,964
7,437.3	3,592
1,636.9	3,629

3.3. Description of the Brazos River

The study area along the Brazos River is a 39.2 mile long stretch located in Fort Bend County, Texas. The Brazos River is characterized by meandering bends and a relatively flat floodplain with levees located on both sides of the river. The average width for the Brazos River reach is around 500 feet and the average slope is 0.016%. The land use classifications for the main channel range from a Manning's n value of 0.035 to 0.042. In the floodplains, the Manning's n values range from 0.06 to 0.12. Figure 3.2 shows the location of the Brazos River as well as the original cross-sectional configuration with some cross section station numbers shown for reference.

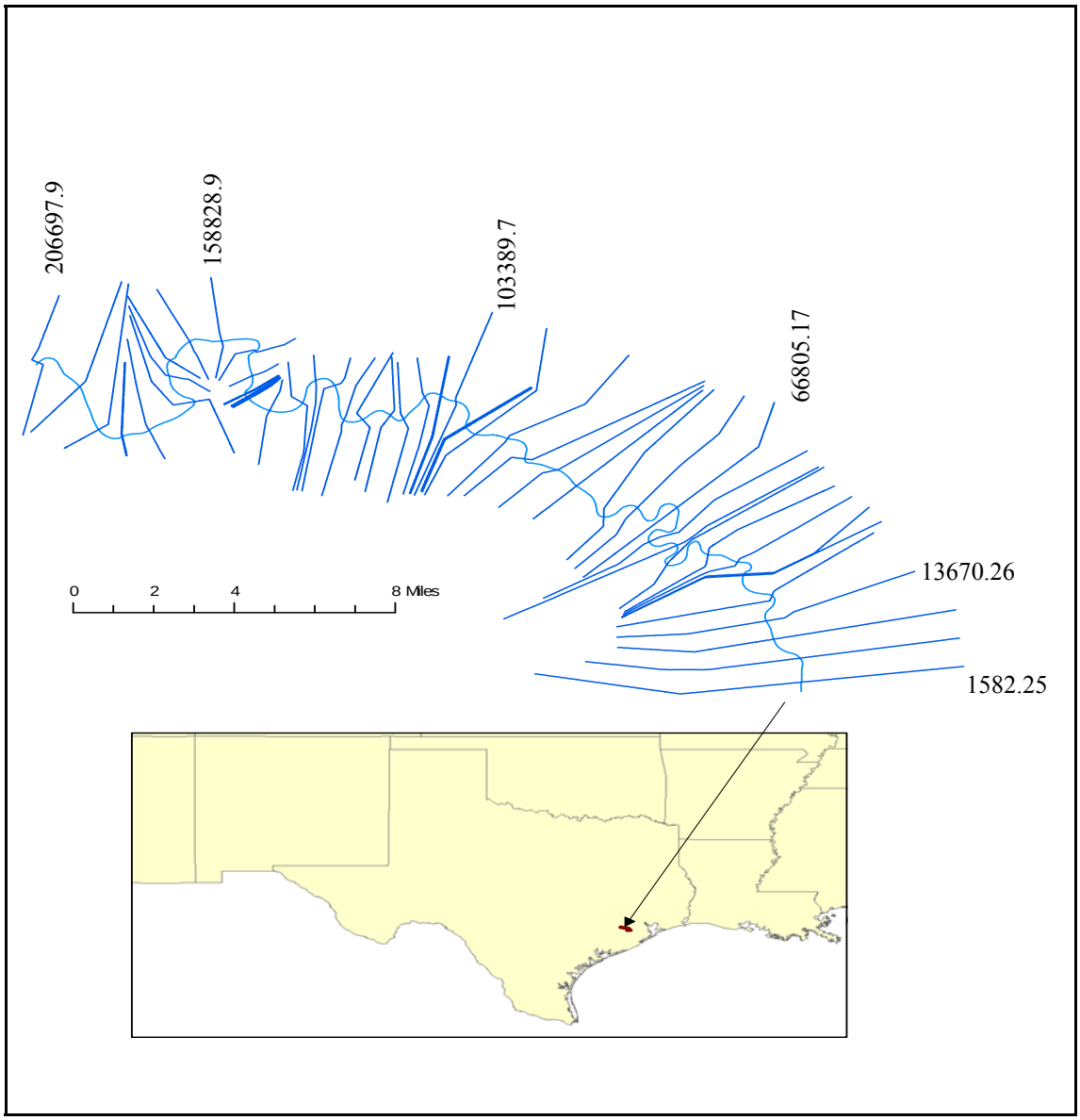

Figure 3.2 Brazos River Study Area

3.3.1. Cross-section and Bridge Data

The original HEC-RAS project file for the Brazos River is obtained from Fort Bend County and consists of data for 53 cross-sections and seven bridges. The original cross-sectional configuration is shown in Figure 3.2. The original 53 cross-sections have an average width of 26,577 feet and average spacing between cross-sections is 3,874 feet.

The following section provides the characteristics of each of the seven bridges located on the reach of the Brazos River being evaluated. For all bridges a drag coefficient, C_d is given as 1.2 and the pier shape coefficient, K as 1.25. A pier shape coefficient of K equal to 1.25 corresponds to a square nose and tail.

FM 723 – Located at station 187388.2 feet.
The FM 723 Bridge Road is 690 feet long and 30 feet wide. The bridge consists of six piers, each 2.5 feet wide.

ASTF Railroad – Located at station 144310.5 feet.
The ASTF Railroad Bridge Road is 900 feet long and 26.9 feet wide. The bridge consists of 4 piers, each 9 feet wide.

SH 90A Southbound – Located at station 143739.9 feet.
The SH 90A Southbound Bridge Road is 990 feet long and 31 feet wide. The bridge consists of 10 piers, the first seven of which are 2.5 feet wide while the remaining three are each 3 feet wide.

SH 90A Northbound – Located at station 143432.3 feet.
The SH 90A Northbound Bridge Road is 1090 feet long and 44 feet wide. The bridge consists of 9 piers, the first seven of which are 2.5 feet wide while the remaining two are each 5.4 feet wide.

SH 99 – Located at station 105636.0 feet.
The SH99 Bridge Road is 1220 feet long and 73 feet wide. The bridge consists of 8 piers, each 5 feet wide.

SH 59 – Located at station 98377.74 feet.
The SH 59 Bridge Road is 1490 feet long and 180 feet wide. The bridge consists of 9 piers, each of which is 3 feet wide.

ATSF Railroad – Located at station 24353.22 feet.

The ATSF Railroad Bridge is 750 feet long and 185 feet wide. The bridge consists of 6 piers, the first has a width of 2.7 feet, the second has a width of 7.4 feet, while the remaining four piers each have a width of 8.5 feet.

3.3.2. Flow Data

The flow data for the 100-year return period are obtained from the HEC-RAS project provided by Fort Bend County. Table 3.1 presents the steady state flow rates assigned at various river stations.

For the 100-year flow, Table 3.2 presents the steady state flow rates assigned at various river stations. A downstream water surface elevation of 57.37 feet was given in the original HEC-RAS project file.

Table 3.2 Flow Rates for Brazos River

Station (ft)	Flow Rate (cfs)
206,697.9	167,000
143,373.8	164,000
1,582.3	158,000

3.4. Light Detection and Ranging Elevation Data

LiDAR (light detection and ranging) data for North Carolina is available from NCFMP and for Texas is available from Fort Bend County. LiDAR data is collected from an aircraft fitted with a laser which measures its distance to the ground, and by tracking the position, pitch and roll of the aircraft the coordinates of the ground surface can be calculated. The laser works with pulses of light that reflect from the earth back to the aircraft. If the pulse reflects off multiple sources, such as vegetation and bare earth, it is common to use the first reflecting pulse as the elevation of vegetation, and the last

reflecting pulse as the elevation of the bare earth (Sanders, 2007). LiDAR data for North Carolina and Texas is characterized by a vertical accuracy of approximately 0.25 meters.

3.5. National Elevation Dataset

National Elevation Dataset (NED) is available for North Carolina, Texas and throughout the contiguous United States from www.seamless.usgs.gov. The NED 30 m DEM is characterized by a horizontal resolution of approximately 30 meters and a vertical accuracy of 7 - 15 meters. The NED 10 m DEM is characterized by a horizontal resolution of approximately 10 meters and a vertical accuracy of approximately 7 meters. NED is a combination of topographic data from several sources including LiDAR and United States Geological Survey (USGS) quadrangle maps (Sanders, 2007). The vertical accuracy of NED is provided by the USGS.

3.6. Integrated Dataset

Because LiDAR or NED does not contain main channel bathymetry, the surveyed cross-section data are integrated with LiDAR to create a new topographic dataset. A detailed description of the process used in creating the integrated DEM is described in Merwade (2007). The integrated DEM is expected produce a more accurate representation of the main channel. The integrated DEM has the same resolution as the LiDAR dataset in the floodplain.

CHAPTER 4. METHODOLOGY

4.1. Introduction

This chapter provides a detailed methodology for creating flood inundation maps using HEC-RAS and FESWMS for Strouds Creek and the Brazos River. For Strouds Creek, 18 cross-sectional modifications and two mesh resolutions are evaluated for four DEMs: integrated, LiDAR, NED 10 m, and NED 30 m resulting in 72 HEC-RAS project files and 8 SMS project files. For the Brazos River, 12 cross-sectional configurations and two mesh resolutions are evaluated for each of the four DEMs resulting in 48 HEC-RAS project files and 8 FESWMS project files. Flow simulation data are taken from the original HEC-RAS project file. For the HEC-RAS simulations, the same process is used for both Strouds Creek and the Brazos River to generate the floodplain. For the FESWMS simulations, the process used to generate the floodplain for Strouds Creek is modified for the Brazos River to accommodate the larger area and to take into account the locations of the levees. A tutorial for using SMS is included in the appendix as a CD-ROM.

4.2. 1D floodplain mapping using HEC-RAS

The original HEC-RAS project data is imported to ArcGIS using HEC-GeoRAS, (available from the website http://www.hec.usace.army.mil/SOFTWARE/hec-ras/hec-georas.html) an ArcGIS extension that provides the user with a set of procedures, tools, and utilities for the preparation of GIS data for input to HEC-RAS and generation of GIS data from HEC-RAS output. The data imported by HEC-GeoRAS consists of a river centerline and cross-sections. Using the HEC-GeoRAS toolbar, bank lines and flow paths are digitized by overlaying an aerial photograph on the data. Bridges and culverts

are then digitized using the aerial photograph as well as the cross-sections as a spatial reference. In HEC-RAS, it is common practice to place cross-sections on either side of bridges or other hydraulic structures. Bridges are placed between these binding cross-sections. Ineffective flow areas, defined as any area that contains water that has zero velocity, and flow obstructions, defined as any area that has no water and no flow, are digitized by referencing the aerial photograph (Merwade, 2006).

To complete the representation of the HEC-RAS project file in ArcGIS, in addition to geometry data such as cross-sections, river centerline, bridges, and left and right banks, HEC-RAS requires Manning's n values and levee locations. The distribution of Manning's n values in the original HEC-RAS project file is used to create a land use polygon in ArcGIS. Similarly, the locations of the levees in the HEC-RAS file are referenced, along with an aerial photograph, to create levees in ArcGIS. Figure 4.1 shows the ArcGIS shape files necessary for a HEC-RAS analysis.

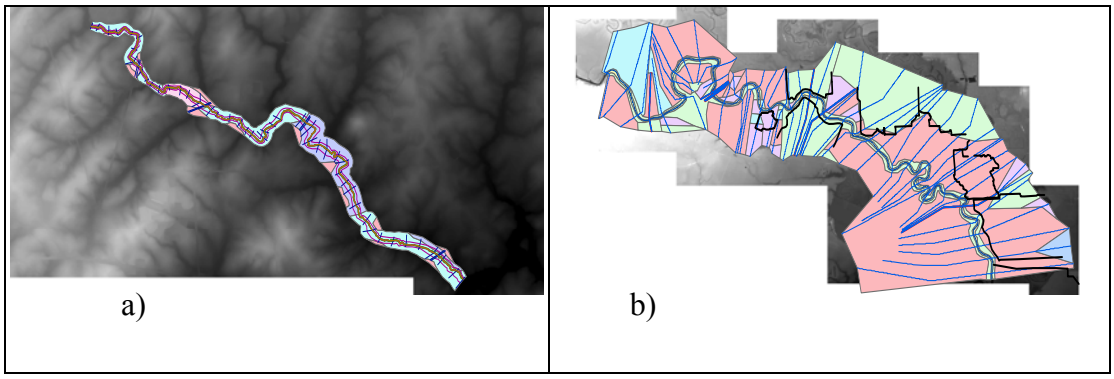

Figure 4.1 HEC-GeoRAS configuration for a) Strouds Creek b) Brazos River

Once the project is set up, different HEC-RAS cross-sectional configurations using the four different topographic datasets are created to show how different cross-sectional configuration and topographic data will affect the resulting floodplain. For Strouds Creek, 18 cross-sectional configurations are analyzed, while for the Brazos River, 12 cross-sectional configurations are analyzed. The cross-sectional modifications for

Strouds Creek and the Brazos River are discussed in sections 4.2.1 and 4.2.2, respectively.

4.2.1. Strouds Creek Cross-sectional Modifications

Table 4.1 provides information for each of the cross-sectional modifications for Strouds Creek. For all cross-sectional modifications, cross-sections on either side of a bridge or culvert and cross-sections that are a flow change location in the original HEC-RAS project file are not removed. The exception to this is the SR3 modification where the cross-sections immediately upstream and downstream of the culverts are removed. For any cross-sectional modification where cross-sections are added, if the original cross-sections are already close together, no cross-sections are added in between the cross-section. In Table 4.1, S represents the original Strouds Creek cross-sections, while any modification with SA shows cross-sections are added, any modification with SR shows cross-sections are removed, and any modification with SI shows cross-sections are located at a specific interval.

Table 4.1 Description of the Cross-sectional Configurations for Strouds Creek

Cross-section Code	Description	# of Cross-sections
S	Original Cross-sections	55
SA1	Double Cross-sections	97
SA2	Triple Cross-sections	139
SA3	Every Curve	76
SR1	Half Cross-sections	34
SR2	One-Third Cross-sections	25
SR3	Without Culvert	53
SR4	Without Cross-section 2	54
SR5	Without Cross-section 3	54
SR6	Without Cross-section 5	54
SR7	Without Cross-section 6	54
SR8	Without Cross-section 7	54
SR9	Without Cross-section 8	54
SR10	Without Cross-section 39	54
SR11	Without Cross-section 41-43	52
SI1	250 ft Interval	94
SI2	500 ft Interval	54
SI3	1000 ft Interval	34

Shown in Figure 4.2 are the locations of cross-sections removed for cross-sectional modifications SR3 to SR11.

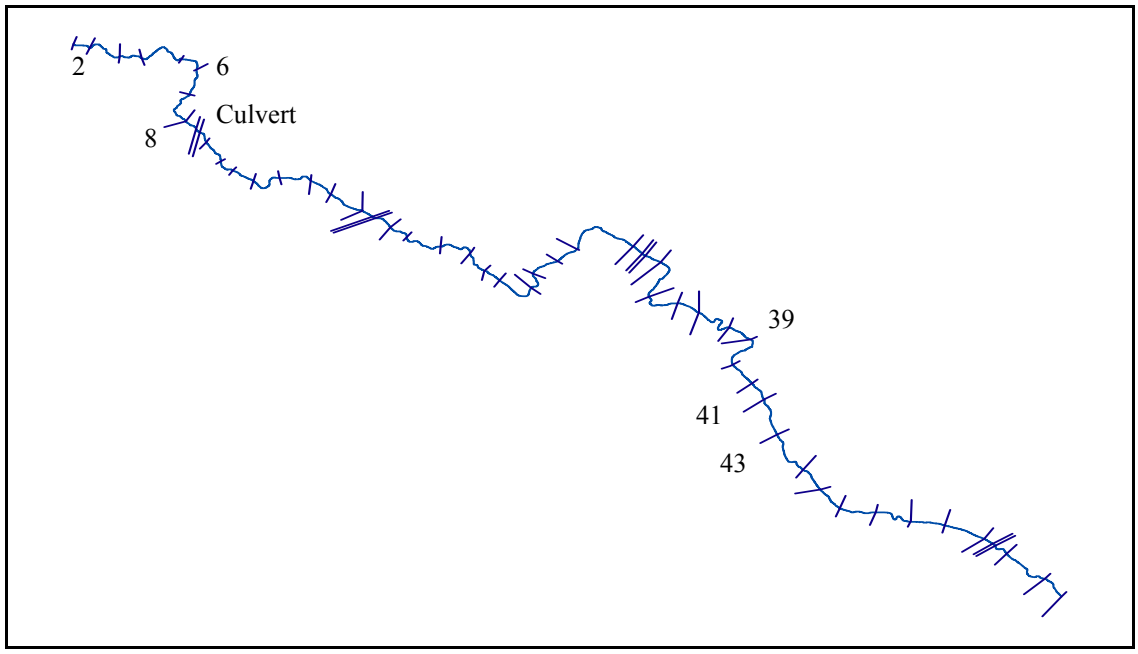

Figure 4.2 Strouds Creek Cross-Sections Removed

Figure 4.3 shows an upstream section of Strouds Creek for 16 cross-sectional modifications and a downstream section of the river for SR10 and SR11. A downstream section is shown for SR10 and SR11 because the cross-sections removed cannot be seen on the upstream section presented for the other 16 cross-sectional modifications. The entire reach of Strouds Creek with original cross-sections is shown in Figure 3.1.

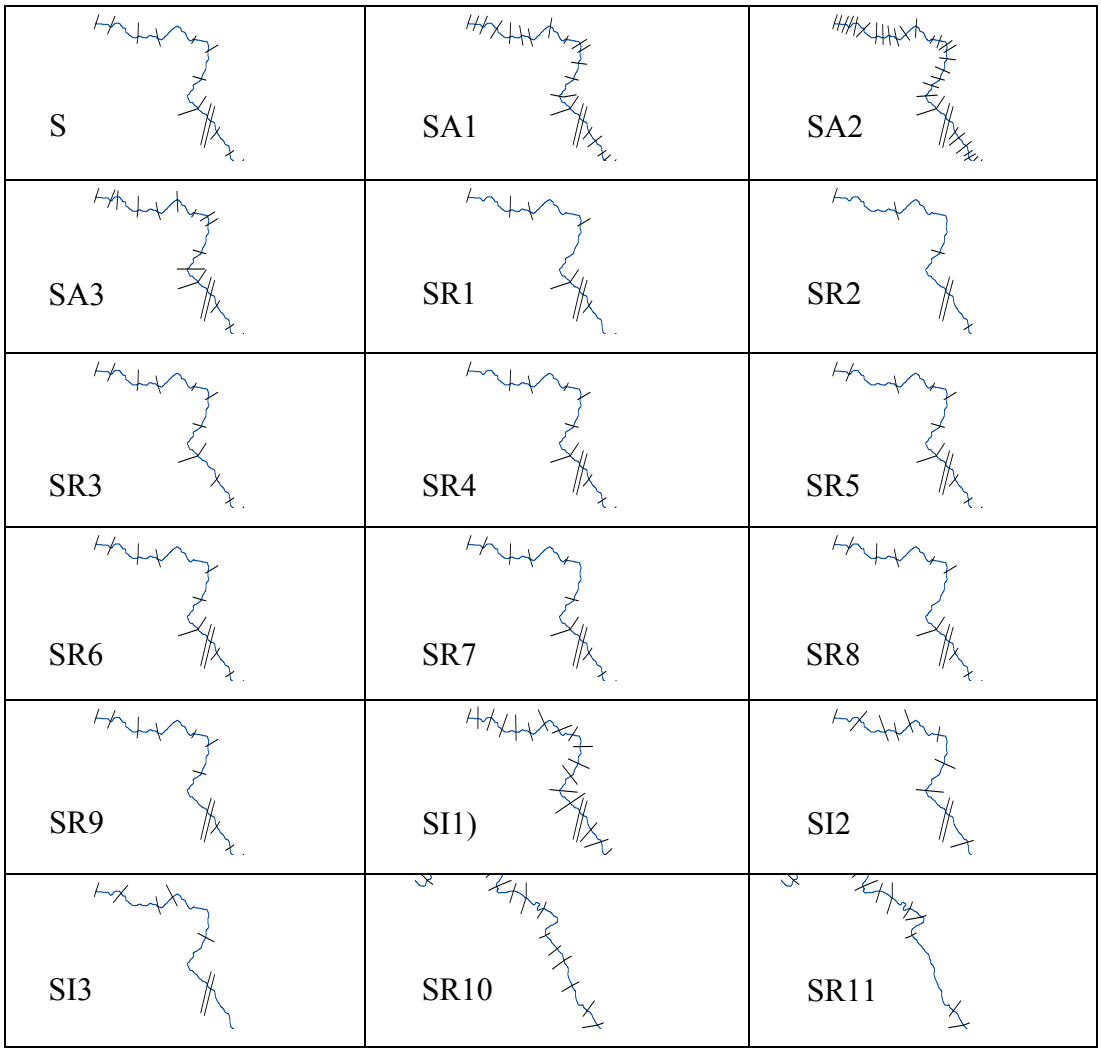

Figure 4.3 Strouds Creek Cross-Sectional Configuration

4.2.2. Brazos River Cross-sectional Modification

Table 4.2 provides information for each of the cross-sectional modifications for the Brazos River. For all cross-sectional modifications, cross-sections on either side of a bridge or culvert and cross-sections that are a flow change location in the original HEC-RAS project file were not removed. For any cross-sectional modification where cross-sections are added, if the original cross-sections are already close together, no cross-sections are added in between the cross-section. In Table 4.2, B represents the original

Brazos River cross-sections, while any modification with BA shows cross-sections are added and any modification with BR shows cross-sections are removed.

Table 4.2 Description of the Cross-sectional Configurations for the Brazos River

Cross-section Code	Description	# of Cross-sections
B	Original Cross-sections	53
BA1	Double Cross-sections	84
BA2	Triple Cross-sections	106
BA3	Every Curve	61
BR1	Half Cross-sections	34
BR2	One-Third Cross-sections	28
BR3	Without Cross-section 2	52
BR4	Without Cross-section 8-9	51
BR5	Without Cross-section 21-22	51
BR6	Without Cross-section 36-37	51
BR7	Without Cross-section 40	52
BR8	Without Cross-section 49-50	51

Shown in Figure 4.4 are the locations of cross-sections removed for cross-sectional modifications BR3 to BR8.

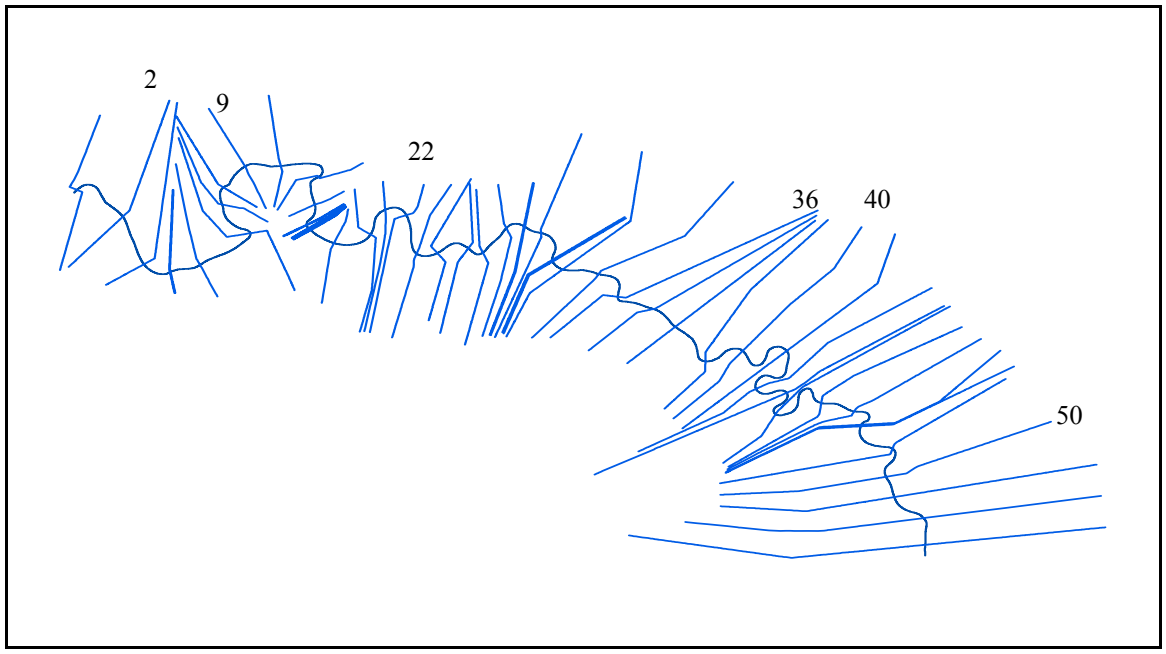

Figure 4.4 Brazos River Cross-Sections Removed

Figure 4.5 shows an upstream section of the Brazos River for nine cross-sectional modifications and a downstream section for cross-sectional modifications BR6, BR7, and BR8. A downstream section is shown for BR6, BR7, and BR8 because the cross-sections removed cannot be shown on the upstream section presented for the other nine modifications. The entire reach of the Brazos River with original cross-sections is shown in Figure 3.2.

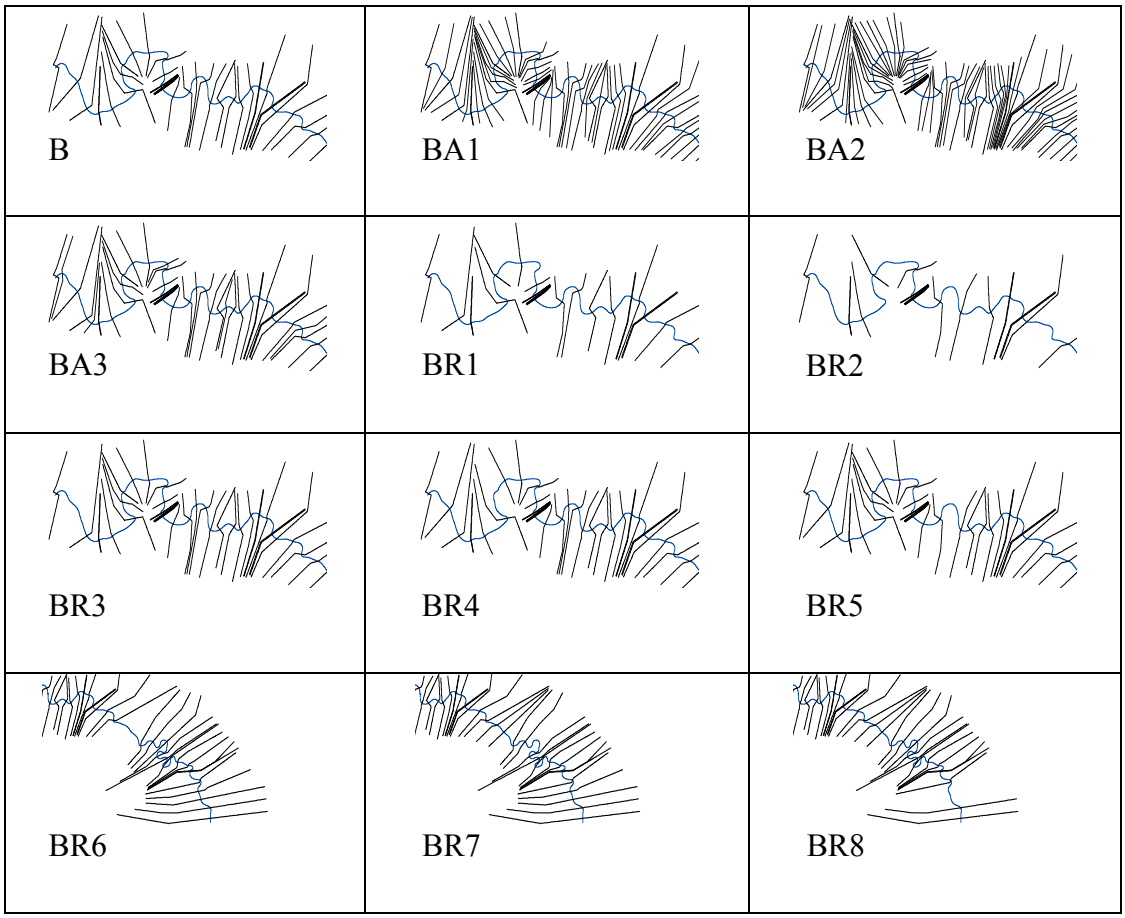

Figure 4.5 Brazos River Cross-Sectional Configuration

4.2.3. Topographic Representation

Each of the cross-sectional modifications are then applied to each of the four digital elevation models (DEM); integrated, LiDAR, NED 10 m, and NED 30 m using the HEC-GeoRAS extension. The HEC-GeoRAS extension assigns elevation data to all shape files created in ArcGIS. To assign elevation data to the levee shape file, the elevations of the levee points are interpolated along the length of the levee to assign elevations at all locations between points. With elevations assigned to each shape file, the information is exported to HEC-RAS for a steady state analysis. For Strouds Creek, 18 HEC-RAS project files are created and for each of the four DEMs and for the Brazos River, 12 HEC-RAS project files are created for each DEM.

4.2.4. Flow Data and Simulation

In HEC-RAS, information must be provided for bridge deck/roadway, bridge piers, and bridge modeling approach. This information is copied from the original HEC-RAS project file. To reduce the number of points along each cross-section to an acceptable level, each cross-section is filtered to 500 points. Flow data available from the original HEC-RAS project is used as input for steady state analysis. Included in the flow data are flow change locations, flow rates, and boundary conditions. Steady state simulation results in HEC-RAS are exported to ArcGIS for preparing flood inundation maps using HEC-GeoRAS.

4.2.5. Flood Inundation Mapping

HEC-GeoRAS is used to create the boundary of the flood extent and the depth of water at each location within the boundary. HEC-GeoRAS creates water depths and floodplain boundaries by subtracting topographic data from water surface elevations imported from HEC-RAS. An area where the water depth is greater than zero is considered to be in the flood boundary. To analyze the data, two variables are taken into consideration. The first being the area of the flood extent and the second being the width of flood along each cross-section in the original HEC-RAS project file. A Visual Basic for Applications (VBA) macro is created to extract the width of the floodplain and these results are compared to results for different digital elevation models, different cross-sectional configurations, as well as the results from the two-dimensional analysis.

4.3. 2D floodplain mapping using FESWMS for Strouds Creek

Surface-water Modeling System (SMS) is a pre and post processor for a suite of two-dimensional finite element and finite difference mesh models. For this study, FESWMS is used as the finite element model to simulate flow conditions for Strouds Creek for the same discharges, land use classifications, and bridge data used in the HEC-RAS simulations.

To create the two-dimensional mesh, the land use shape file created in ArcGIS is opened in the GIS module of SMS. Using the GIS module, the land use shape file is converted to a feature object for use in the Map module of SMS. In the map module, polygons are created for each land use classification based on a Manning's n value. One of the goals when creating the mesh is to create uniform mesh elements. To do this, most of the Manning's n value polygons are subdivided. For most polygons, the patch meshing type is selected. The patch meshing type provides rectangular elements which are semi-uniform. One of the requirements for the patch meshing type is a polygon with exactly four nodes. For any polygons with only three nodes, a paving meshing type is selected. The paving meshing type generally creates triangular elements. Material type, or Manning's n value, is also assigned in the map module. With the material type and meshing type selected, the map is converted to a mesh.

4.3.1. Strouds Creek Mesh Resolution

For each of the four digital elevation models, a map with vertices at 10 feet intervals and a map with vertices at 20 foot intervals are created. Figure 4.6 shows the 10 foot and 20 foot mesh resolutions for a section of Strouds Creek.

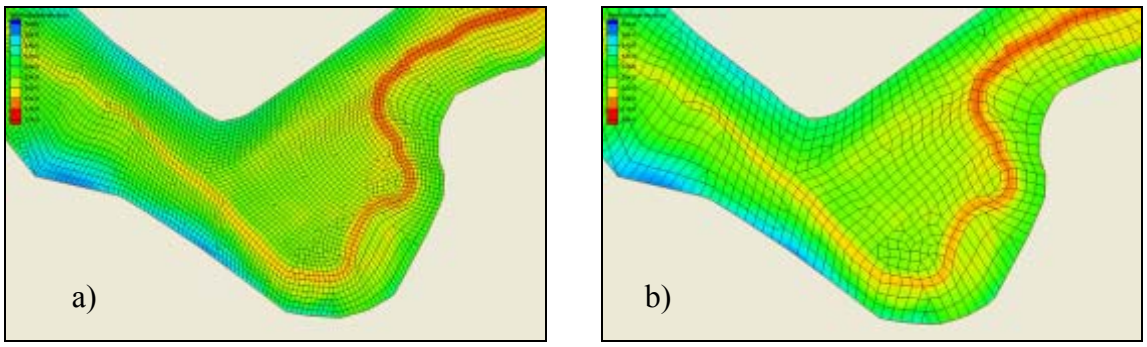

Figure 4.6 Strouds Creek mesh resolution in SMS a) 10 foot b) 20 foot

4.3.2. Topographic Representation

The next step in the two-dimensional floodplain mapping process involves using ArcGIS to convert the DEMs into an acceptable file type for use in SMS. The DEMs are converted into ASCII (American Standard Code for Information Interchange) format using Arc Toolbox in ArcGIS. The ASCII format is recognized by SMS whereas the raster or TIN format used in GIS is not recognized by SMS. The ASCII file is opened in the Scatter Module of SMS. The resulting scatter set will provide (x,y,z) data for all the elevation points in a given elevation dataset. This process is followed for each of the topographic datasets considered. In the scatter module, the ASCII elevation file is linearly interpolated to assign an elevation to each node in the mesh.

4.3.3. Flow Data and Simulation

In the mesh module, material properties, including an eddy viscosity of 5 ft^2/s are assigned. According to FESWMS (2002), increasing the eddy viscosity causes velocity gradients to be reduced increasing the chance of a successful simulation. According to a USGS study of the Flint River at Albany, Georgia, eddy viscosity can be used as an important parameter in calibrating the model to obtain correct water surface elevations. Using Equation 2.18 and Equation 2.19, the eddy viscosity for Strouds Creek should be in the range of 5 ft^2/s for a water depth ranging between 5 and 12 feet and an average channel slope of 0.56%. Also in the mesh module, an upstream flow rate and a downstream water surface elevation are assigned. Because the Strouds Creek HEC-RAS project file has six different flow rates at different sections along the reach being considered, the land use file was divided into six separate meshes. Flow rates in SMS are assigned according to Table 3.1, which shows the flow rates given in the HEC-RAS project file, and the flow change locations are shown in Figure 3.1. Each mesh is then subdivided to improve the chances of a successful FESWMS simulation and to reduce the time for each simulation. The downstream water surface elevation for the entire reach of Strouds Creek being studied is given in the HEC-RAS project file to be 478.64 feet. FEWSMS spin down is used to determine the final solution for the given boundary

conditions. When using FESWMS, an initial condition must be specified such that all nodes in the mesh are initially wet. With the user specified initial conditions, FESWMS spin down incrementally decreases the downstream water surface elevation until the specified boundary condition is reached. When the most downstream mesh section successfully converged to a steady state solution for this water elevation, the upstream water surface elevation of this section is recorded and used as the downstream water surface elevation boundary condition for the next section upstream. This process is repeated for each section. Due to trouble with model convergence on the section which contained the culvert, SMS results only consider the portion of Strouds Creek downstream of the culvert. When SMS cannot successfully spin down the water surface elevation to the desired value, the model has not converged for the given parameters.

4.3.4. Flood Inundation Mapping

To determine the width of the floodplain at specified cross-sections to compare with the results from the one-dimensional HEC-RAS simulation, the floodplain results from SMS are exported for use in ArcGIS. To do this, a contour of zero water surface elevations was created in the mesh module. This contour, when converted to the map module, represented the boundary of the floodplain. The contour was then saved as a shape file and opened in ArcGIS. In ArcGIS, the shape files for each section were merged to create a floodplain for the entire length of Strouds Creek. A VBA macro was created to extract the width of the floodplain at original HEC-RAS cross-section locations, and these results are compared with results for different digital elevation models, different mesh spacing, as well as the results from the one-dimensional analysis.

4.4. 2D floodplain mapping using FESWMS for the Brazos River

The process to complete the two-dimensional analysis of the floodplain for the Brazos River is intended to be similar to that done for Strouds Creek, but due to the large area of the floodplain and locations of the levees, only a nine mile long upstream section of the

river is analyzed with FESWMS. The entire reach could not be analyzed at an acceptable mesh resolution because the number of mesh elements produced is too large for the computing capabilities of the computer used in this study. The nine mile section of the river is selected such that the mesh resolution would be refined enough to accurately model the flow through the compound channel and no levees are split in that section. The levees, as a general trend, run parallel to the river before branching off perpendicular to the river. If the levees are split and modeled in SMS, the resulting floodplain will always show flow on both side of the levees because there is no upstream levee boundary keeping the flow from the floodplains.

Instead of using the GIS land use shape file to create the basis for the mesh to be used in SMS, a scatter file created from the elevation ASCII file is used. In this study for the Brazos River, a 500 foot interval is selected because of the large area of the floodplain. The 500 foot spacing scatter file is then converted to a mesh. The advantage of using this technique is that an ideal mesh is created. Each mesh element created is either a perfect square or a right triangle. In the vicinity of the main channel, the mesh is refined to create elements with mesh spacing less than 500 feet. The Brazos River main channel is deep and when the mesh is not refined in the vicinity of the main channel, important elevation data is lost within the main channel. If the mesh is not refined in the main channel, the flow through the main channel will decrease causing more flow to be routed through the floodplains and will produce unrealistic results for floodplain analysis. After creating the mesh, land use Manning's n values are assigned. Manning's n values are assigned as either floodplain or main channel. Floodplain zones are assigned a Manning's n value of 0.12 while the main channel is assigned a Manning's n value of 0.05. The Manning's n values selected are representative values given in the HEC-RAS project file.

4.4.1. Brazos River Mesh Resolution

For each of the four digital elevation models, maps with main channel vertices at 125 and 250 foot intervals are created. Figure 4.7 shows the 125 and 250 foot main channel mesh resolution for the nine mile section of the Brazos River being considered.

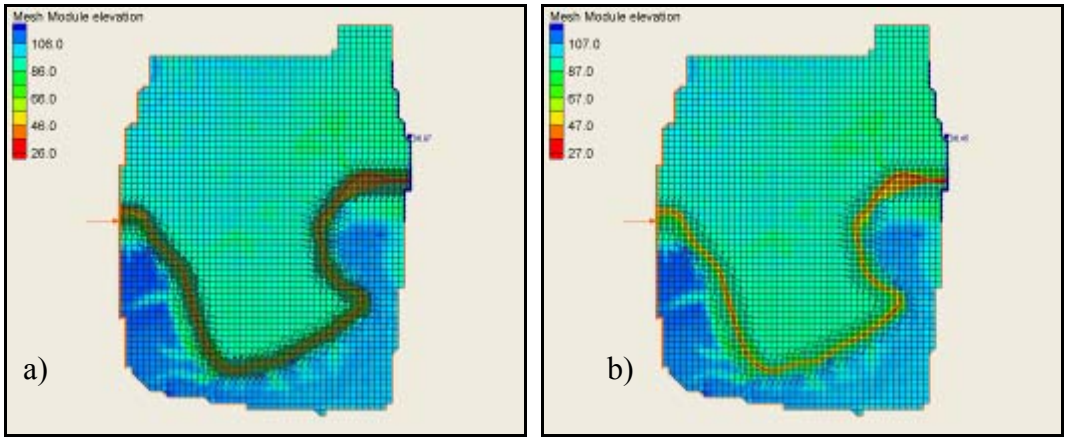

Figure 4.7 Brazos River mesh resolution in SMS a) 125 foot b) 250 foot

4.4.2. Topographic Representation

The next step in the two-dimensional floodplain mapping process involves assigning elevation data to the mesh. The process is the same as what is done for Strouds Creek and can be seen in Section 4.3.2.

4.4.3. Flow Data and Simulation

With the mesh created, a steady state solution was selected and all material properties and turbulence parameters were assigned. An eddy viscosity of 200 ft^2/s is selected because this value allowed for model convergence for each of the four topographic datasets for both the mesh resolutions considered. Using Equation 2.18 and Equation 2.19, the eddy viscosity for the Brazos River should be between 10 and 30 ft^2/s. For the integrated DEM, the model will converge for an eddy viscosity of 25 ft^2/s, but for the lower resolution DEMs, the model does not converge for an eddy viscosity lower than 200 ft^2/s.

According to FESWMS (2002), large increases in eddy viscosity raise upstream water surface elevations far less than large increases in roughness coefficients for a channel of uniform width, but do reduce velocity gradients increasing the chance for a successful simulation. According to a study performed by Zanichelli et al. (2004), eddy viscosities of close to 150 ft^2/s are acceptable for deep channels. To be consistent between each topographic dataset, the value of eddy viscosity is selected such that each topographic dataset can achieve model convergence. An upstream flow rate and downstream water surface elevation boundary conditions are assigned, and FEWSMS spin down is used to converge to a successful simulation. For this section of the Brazos River, the downstream water surface is determined to be 86.97 feet using the HEC-RAS project file. The flow rate, also given in the HEC-RAS project file, is 167,000 cfs.

4.4.4. Flood Inundation Mapping

To determine the width of the floodplain at specified cross-sections to compare with the results from the one-dimensional HEC-RAS simulation, the same process is used as that described for Strouds Creek in Section 4.3.4.

CHAPTER 5. RESULTS

5.1. Introduction

The results from steady flow hydraulic modeling and flood inundation mapping are presented in this chapter for both Strouds Creek and the Brazos River. For both rivers, inundation area, average width of inundation along the original cross-sections, and percent change in area using the integrated DEM as the benchmark are presented for each DEM. To compare the effect of geometry on the one-dimensional model, 18 cross-sectional configurations for Strouds Creek and 12 cross-sectional configurations for the Brazos River are evaluated by determining area of inundation and average inundation width along the original cross-sections for each DEM. To compare the effect of geometry on the two-dimensional model, mesh resolutions of 10 and 20 feet for Strouds Creek and 125 and 250 feet for the Brazos River are evaluated for each DEM by determining inundation area and average width of inundation. The results from the HEC-RAS and FESWMS simulations are then compared.

5.2. Effect of Topography on one-dimensional hydraulic model

In this section, four DEMs are evaluated for hydraulic modeling and floodplain mapping using the original 55 HEC-RAS cross-sections for Strouds Creek and the original 53 cross-sections for the Brazos River. The extent of inundation is measured by the area of inundation and the average width of inundation along the original cross-sections.

5.2.1. Strouds Creek

Table 5.1 presents the inundation area, the average width of inundation along the cross-sections, and the percent change in inundation area using the results from the integrated

DEM as the benchmark. The percent change in inundation area is shown in parenthesis for each DEM evaluated.

Table 5.1 Inundation for Original Cross-sections

	NED 30 m	NED 10 m	LiDAR	Integrated
Area (mi^2) (% change)	0.199 (64.35)	0.178 (46.67)	0.145 (19.87)	0.121 (0.00)
Average Width (ft)	297.33	264.29	234.40	185.46

The results of this table show that the integrated DEM produces the least amount of inundation area and the least average width of inundation, followed by the LiDAR, NED 10 m and NED 30 m DEMs. Overall, the area of inundation increases with decreasing DEM resolution. Both the integrated and LiDAR DEMs have the same resolution data in the floodplain, while the integrated DEM is a more accurate representation of the topography in the main channel. The NED 10 m DEM has a horizontal resolution of approximately 30 feet and the NED 30 m DEM has a horizontal resolution of approximately 90 feet. The percentage increase in area is 64.35 % for the NED 30 m DEM when compared to the integrated DEM.

Figure 5.1 further shows the difference in inundation area for each of the four DEMs being considered. Figure 5.1 shows a magnified image of the floodplain developed using the original cross-sections and each DEM.

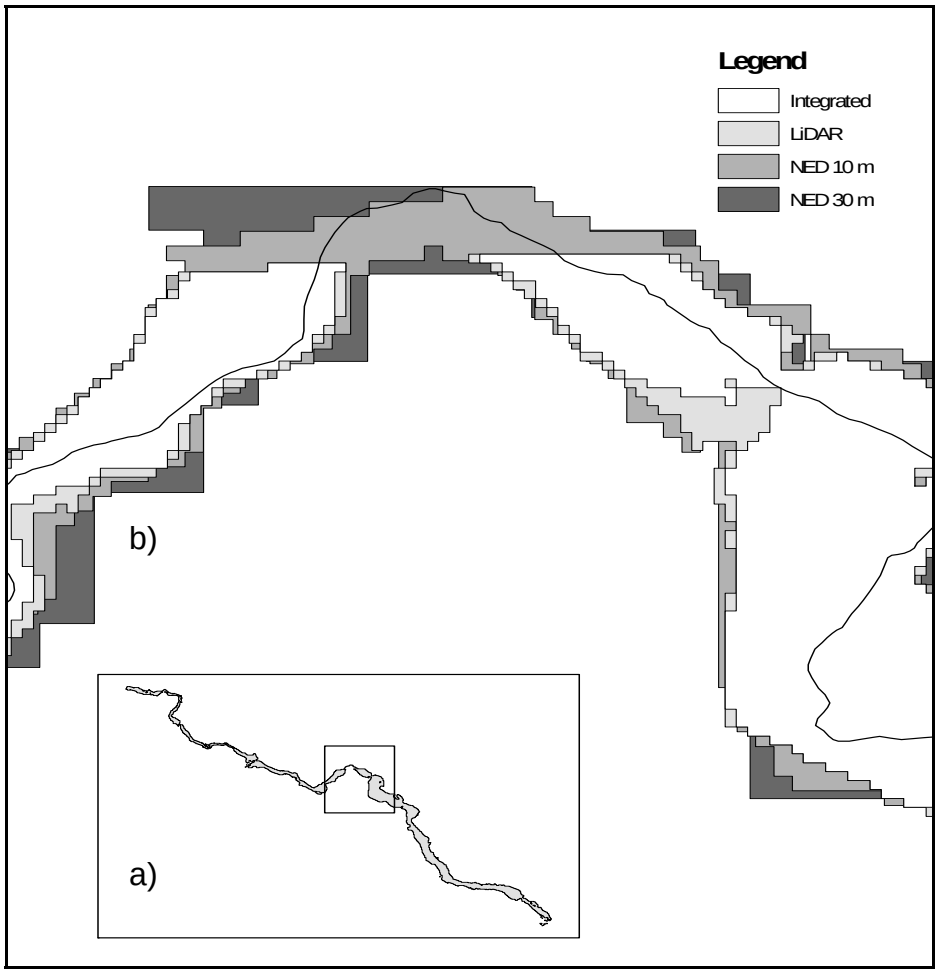

Figure 5.1 Inundation Boundary for a) Entire Reach; b) Magnified to a Bend in the River

The inundation extent for the integrated DEM shows that there are two areas, one near the upstream section of the reach and one near the midpoint of the reach, where no flooding is shown to take place. The area where no flooding is shown to take place near the midpoint of the reach is magnified in Figure 5.1. For the LiDAR DEM, the upstream area where no flooding occurred using the integrated DEM is now flooded, whiles the area near the midpoint of the reach remains without flooding. For both the NED 10 m DEM and NED 30 m DEM, both areas shown previously to have no flooding are now flooded. In looking at the NED 30 m DEM, there is a clear change in resolution, with the floodplain appearing as a series of large blocks.

The horizontal resolution for both the integrated DEM and the LiDAR DEM are the same in the floodplain meaning a change in inundated area is due to a change in the representation of the main channel. This change can be seen through a representative HEC-RAS cross-section station 7986.1 feet for both the integrated and LiDAR DEMs shown in Figure 5.2. The shape of the cross-sections are nearly identical, with the exception being that the main channel for the integrated DEM is deeper than that of the LiDAR DEM. Because LiDAR cannot penetrate deep water, in the LiDAR DEM cross-section, the main channel invert is around 515 feet while the integrated DEM cross-section has a main channel invert below 510 feet. As a result, the area of the main channel is larger for the integrated DEM which means more flow is routed through the main channel and less will flow in the floodplains. When less flow is routed through the floodplains, the area of inundation is less. The difference in inundation extent can also be seen in the fact that the water surface elevation for the LiDAR cross-section is higher than that of the integrated DEM cross-section. The water surface elevations are 520.28 and 521.23 feet for the integrated and LiDAR DEMs.

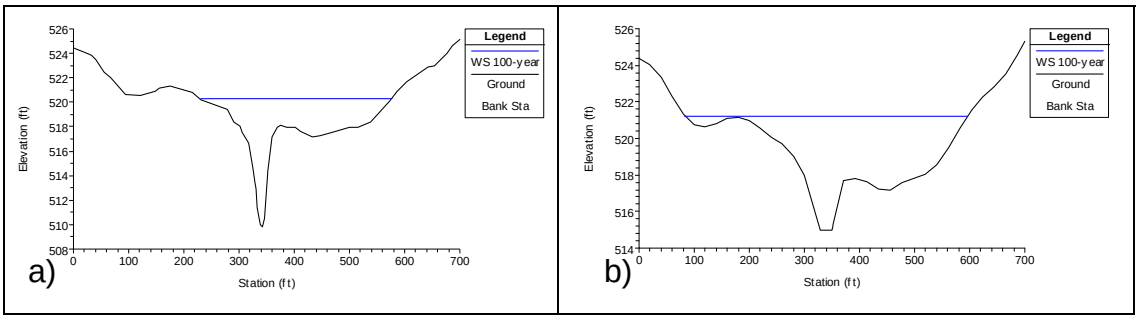

Figure 5.2 Cross-section Station 7986.1 for the a) Integrated; b) LiDAR DEM

When the resolution is further decreased, as is the case for the NED 30 m DEM and the NED 10 m DEM, the main channel definition is further reduced, and the extent of inundation becomes larger. The width of the main channel of Strouds Creek is approximately 30 feet, meaning when the resolution of the DEM exceeds 30 feet, each cross-section sampled will have no more than one point located in the main channel. In

the case of the NED 30 m DEM, which has a horizontal resolution of approximately 90 feet, no points in the main channel may be sampled for some cross-sections.

5.2.2. Brazos River

The overall results for the Brazos River with respect to inundation area and average width of inundation for different DEMs are similar to Strouds Creek and are presented in Table 5.2.

Table 5.2 Inundation for Original Cross-sections

	NED 30 m	NED 10 m	LiDAR	Integrated
Area (mi^2) (% change)	109.81 (25.66)	109.34 (25.12)	104.68 (19.79)	87.39 (0.00)
Average Width (mi)	4.228	4.216	4.228	3.815

The results of Table 5.2 show that the percentage increase in inundation area from the integrated to the NED 30 m DEM is 25.66 % compared to 64.35 % for Strouds Creek. This is due to the comparatively small channel area when compared to the floodplain area. For Strouds Creek, a large amount of the flow is routed through the channel causing the topographic representation of the main channel to become very important. For Brazos River, the 100-year flow routs most of the flow through the floodplain causing the topographic representation of the main channel to become less important.

Figure 5.3 shows the difference in inundation boundary for each of the four DEMs being considered for the original cross-section locations. Locations of the levees are also shown on the figure.

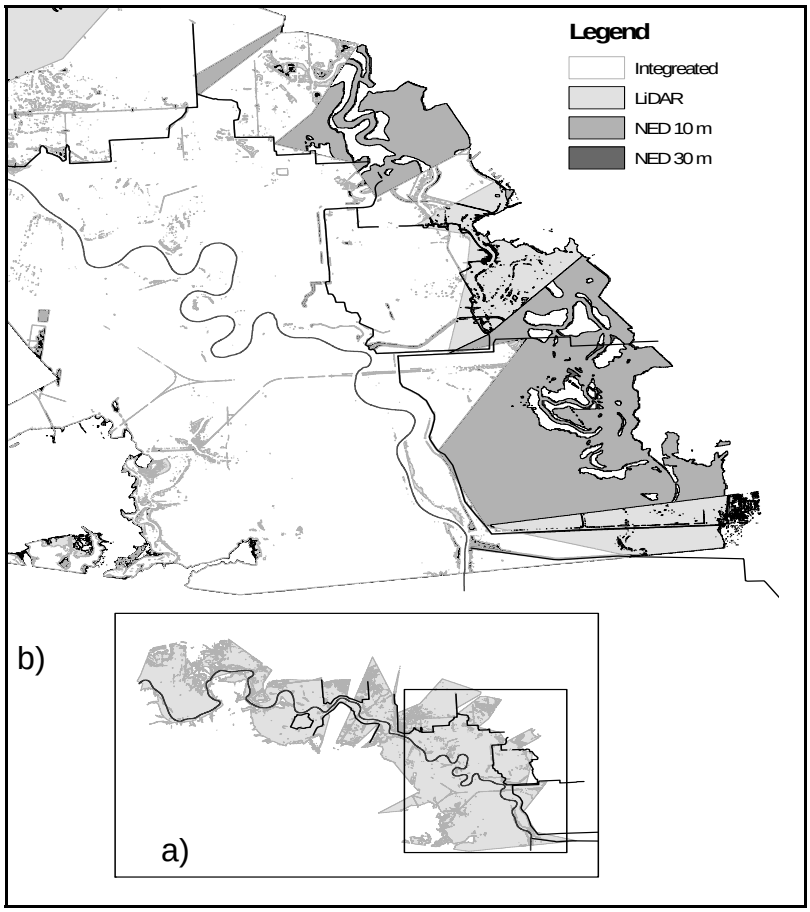

Figure 5.3 Inundation Boundary for a) Entire Reach; b) Magnified to the Levees

The section of the Brazos River shown in Figure 5.3 is a downstream section of the river in which the levees are shown to block flow into the floodplains for the higher resolution DEMs while the lower resolution DEMs show levee overtopping and flow being routed into the floodplains. There is also a noticeable difference in the inundation extent upstream of the section shown in Figure 5.3 between the integrated and LiDAR DEMs in which the LiDAR DEM shows overtopping of some levees resulting in a larger inundation area. The difference in inundation over the entire length of the reach being considered between the integrated and LiDAR DEMs is presented in Figure 5.4.

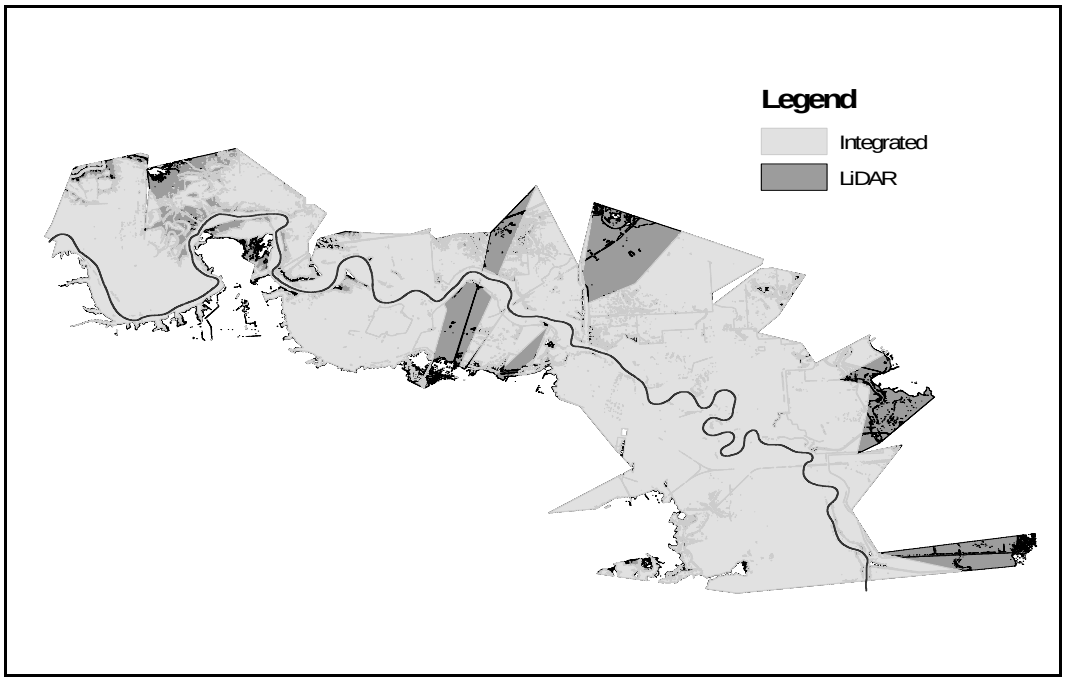

Figure 5.4 Inundation Boundary for Original Cross-sections for the Integrated and LiDAR DEMs

The change in representation of the main channel causing levee overtopping at some locations can be seen through a representative HEC-RAS cross-section station 143373.8 feet for both the integrated and LiDAR DEMs in Figure 5.5. The main channel invert for the integrated DEM cross-section is approximately 25 feet while the main channel invert for the LiDAR DEM cross-section is approximately 50 feet. The difference in inundation extent can be seen in the fact that the water surface elevation for the LiDAR DEM cross-section is 84.53 feet while the integrated DEM cross-section shows a water surface elevation of 81.72 feet. The difference in water surface elevations is enough to cause overtopping of the levees at some locations.

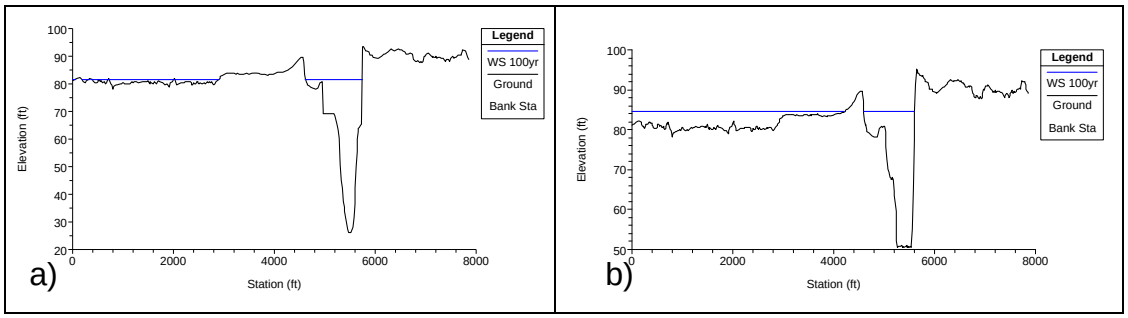

Figure 5.5 Cross-section Station 143373.8 for a) Integrated; b) LiDAR DEM

5.3. Effect of Geometry on one-dimensional hydraulic model

In this section, four DEMs are evaluated for hydraulic modeling and floodplain mapping using 18 HEC-RAS cross-sectional modifications for Strouds Creek and 12 cross-sectional modifications for the Brazos River as discussed in sections 4.2.1 and 4.2.2. The extent of inundation is measured by the area of inundation and the average width of inundation along the original cross-sections.

5.3.1. Strouds Creek

Table 5.3 provides the area extent of inundation for each of the 18 cross-sectional configurations. The percent change in inundation area is shown in parenthesis. The percent change in inundation area is in reference to the original cross-sectional configuration for each DEM.

Table 5.3 Inundation Area (mi^2) (% Change)

	NED 30 m	NED 10 m	LiDAR	Integrated
S	0.199 (0.00)	0.178 (0.00)	0.145 (0.00)	0.121 (0.00)
SA1	0.203 (1.73)	0.178 (0.26)	0.154 (5.82)	0.129 (6.19)
SA2	0.203 (2.08)	0.179 (0.55)	0.158 (8.54)	0.132 (9.36)
SA3	0.201 (1.04)	0.179 (0.92)	0.156 (7.64)	0.131 (8.44)
SR1	0.197 (-1.21)	0.174 (-1.82)	0.132 (-8.99)	0.110 (-9.52)
SR2	0.187 (-5.88)	0.168 (-5.28)	0.118 (-18.59)	0.098 (-19.15)
SR3	0.198 (-0.69)	0.177 (-0.55)	0.131 (-9.86)	0.111 (-8.27)
SR4	0.199 (0.00)	0.178 (-0.02)	0.145 (0.07)	0.121 (-0.33)
SR5	0.199 (0.00)	0.178 (-0.07)	0.145 (-0.11)	0.121 (-0.08)
SR6	0.197 (-1.04)	0.177 (-0.22)	0.144 (-0.58)	0.119 (-1.42)
SR7	0.198 (-0.52)	0.177 (-0.11)	0.143 (1.62)	0.120 (-1.17)
SR8	0.199 (0.00)	0.177 (-0.20)	0.145 (0.09)	0.121 (-0.08)
SR9	0.198 (-0.69)	0.177 (-0.15)	0.143 (-1.39)	0.120 (-1.26)
SR10	0.199 (0.00)	0.178 (0.26)	0.142 (-1.97)	0.118 (-2.34)
SR11	0.199 (0.00)	0.178 (0.00)	0.144 (-1.07)	0.12 (-1.27)
SI1	0.203 (2.08)	0.180 (1.14)	0.157 (7.81)	0.132 (8.85)
SI2	0.199 (0.17)	0.179 (0.66)	0.149 (2.75)	0.124 (2.04)
SI3	0.193 (-3.11)	0.177 (-0.29)	0.136 (-6.39)	0.112 (-7.86)

From Table 5.3, it is seen that the integrated DEM produced the least area of inundation for each of the cross-section modifications, followed by the LiDAR DEM, the NED 10 m DEM, and the NED 30 m DEM. It is also seen that the cross-sectional modifications where cross-sections are added (SA1, SA2, SA3, SI1) produce the largest area of inundation, while the least area of inundation is produced from the cross-sectional modifications where cross-sections are removed (SR1, SR2, SI3). The exception to this rule is seen in the SR3 modification for the integrated and LiDAR DEMs. For this modification, the cross-sections on either side of a culvert are removed. The lesser area shown in Table 5.3 for the SR3 modification is caused by the model producing no inundation area upstream of the culvert. This result shows the importance of including cross-sections on either side of a hydraulic structure in one-dimensional hydraulic modeling.

The results of Table 5.3 also suggest that increasing or decreasing the number of cross-sections for a high resolution DEM has a larger affect than increasing or decreasing the number of cross-sections for a lower resolution DEM. The SR2 cross-sectional

modification can be used as an example. For both the NED 30 m and NED 10 m DEMs, the percent decrease in inundation area is below 6%, while the percent decrease in inundation area for the LiDAR and integrated DEMs is nearly 20%. Figure 5.6 and Figure 5.7 show the effect of increasing or decreasing the number of cross-sections on the resulting floodplain for the integrated DEM and NED 30 m DEM, respectively By adding cross-sections, as is done in the SA1 cross-sectional modification, the area shown not to be flooded in for the integrated DEM is now flooded in Figure 5.6. By reducing the number of cross-sections, as is done in the SR1 and SR2 cross-sectional modifications, the floodplain becomes further degraded. Figure 5.7 shows only a small change in the inundation area for the NED 30 m DEM when the cross-sectional configuration is altered. The results of the LiDAR DEM simulations are similar to those of the integrated DEM while the results of the NED 10 m DEM simulations are similar to those of the NED 30 m DEM.

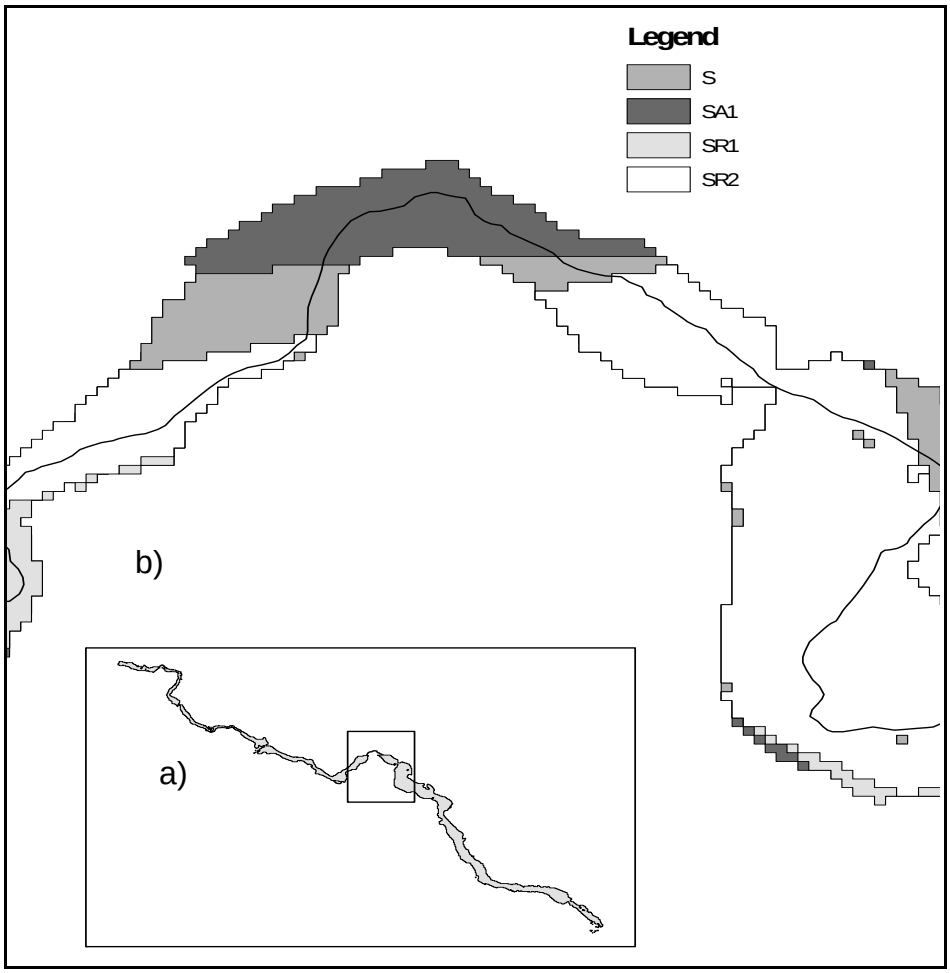

Figure 5.6 Inundation Boundary for the Integrated DEM for a) Entire Reach; b) Magnified Section for Four Cross-Sectional Modifications

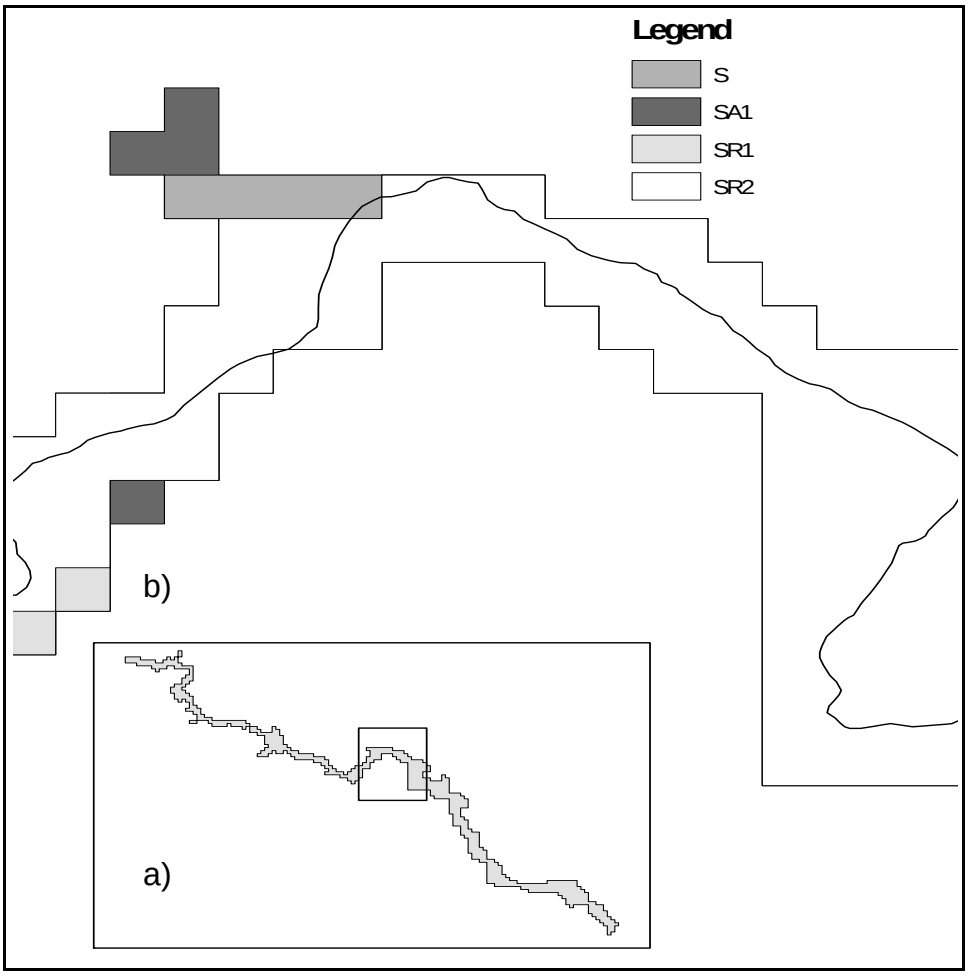

Figure 5.7 Inundation Boundary for the NED 30 m DEM for a) Entire Reach; b) Magnified Section for Four Cross-Sectional Modifications

To further show the effect of cross-sectional modifications in a one-dimensional HEC-RAS simulation, Table 5.4 presents the average width of inundation along the original 55 cross-sections for each DEM being evaluated. The results of this table show that decreasing the number of cross-sections will decrease the average width of inundation while increasing the number of cross-sections will increase the average width of inundation. For each of the DEMs being considered, the least average width of inundation is produced by a cross-sectional configuration in which a significant number of cross-sections are removed. Conversely, the maximum average width of inundation is produced by a cross-sectional modification in which a significant number of cross-

sections are added. The results of Table 5.4 correspond well to the results of Table 5.3 in which the areas of inundation for each cross-sectional modification are presented.

Table 5.4 Average Width of Inundation (ft)

	NED 30 m	NED 10 m	LiDAR	Integrated
S	297.33	264.29	234.40	185.46
SA1	301.75	262.31	234.00	184.89
SA2	300.58	263.42	235.62	190.39
SA3	299.44	263.83	234.12	186.15
SR1	297.62	263.79	217.47	171.75
SR2	278.76	262.86	200.42	156.99
SR3	289.27	258.81	205.78	167.03
SR4	297.33	264.29	234.40	184.68
SR5	297.33	264.29	232.89	184.68
SR6	295.79	264.29	233.22	183.89
SR7	297.33	264.84	231.04	182.96
SR8	297.33	263.63	234.81	184.60
SR9	295.54	264.29	232.29	183.62
SR10	297.33	264.79	229.91	180.62
SR11	297.33	264.29	233.18	183.01
SI1	295.62	264.95	246.56	193.34
SI2	293.89	265.36	237.32	186.13
SI3	281.44	261.83	227.00	175.68

By removing one or a series of cross sections from the original cross-sectional configuration, as is done in cross-sectional modifications SR4 to SR11, the width of inundation only changes in the immediate vicinity of the cross-sections(s) being removed. For the higher resolution DEMs, removing one cross-section results in a maximum decrease in inundation width equal to 100 %, meaning the width of inundation is zero along the cross-section removed. Removing cross-sections(s) at bend in the river results in the largest change in inundation width although no change in inundation is seen sufficiently far up or downstream. Cross-sectional modification SR10 removes three consecutive cross-sections on a relatively straight portion of the river but results in less change in inundation width than removing one cross-section located on a bend. For the lower resolution DEMs, the maximum decrease in inundation width due to removing one or a series of cross-sections is 42 %.

5.3.2. Brazos River

The results of the effect of change in cross-section configuration for the Brazos River are presented in Table 5.5 for each DEM.

Table 5.5 Inundation Area (mi^2) (% Change)

	NED 30 m	NED 10 m	LiDAR	Integrated
B	109.81 (0.00)	109.34 (0.00)	104.68 (0.00)	87.39 (0.00)
BA1	109.00 (-0.74)	108.02 (-1.20)	104.04 (-0.61)	90.84 (3.95)
BA2	108.67 (-1.04)	107.92 (-1.29)	99.89 (-4.57)	85.65 (-1.99)
BA3	108.67 (-1.04)	108.23 (-1.01)	103.15 (-1.46)	86.03 (-1.55)
BR1	107.01 (-2.55)	106.74 (-2.37)	104.82 (0.13)	86.16 (-1.41)
BR2	103.80 (-5.48)	103.9 (-4.96)	97.17 (-7.18)	83.78 (-4.13)
BR3	109.72 (-0.08)	109.23 (-0.10)	104.68 (0.00)	87.24 (-0.17)
BR4	109.72 (-0.09)	109.28 (-0.06)	104.70 (0.02)	86.86 (-0.61)
BR5	109.65 (-0.15)	109.15 (-0.17)	104.53 (-0.14)	86.91 (-0.54)
BR6	110.67 (0.78)	110.24 (0.82)	105.96 (1.22)	87.83 (0.51)
BR7	109.61 (-0.18)	109.11 (-0.21)	105.79 (1.06)	87.04 (-0.39)
BR8	109.16 (-0.60)	108.48 (-0.78)	105.71 (0.99)	88.60 (1.39)

From Table 5.5, it is seen that the integrated DEM produced the least area of inundation for each of the cross-sectional modifications, followed by the LiDAR DEM, the NED 10 m DEM, and the NED 30 m DEM, which is similar to the results seen in Strouds Creek. This table also shows that the largest inundated area for the integrated DEM is produced by the BA1 cross-sectional modification, while the largest inundated area for the other three DEMs is produced for the BR6 modification. When cross-section placement is changed in the vicinity of levees, a large change in inundation area is seen. This large change is due to the process by which HEC-GeoRAS linearly interpolates the floodplain boundary between adjacent cross-sections. For the Brazos River reach being analyzed, the levees generally run parallel to the river before branching off perpendicular, making a modified "U" shape as is seen in Figure 5.3. If a cross-section is removed from the section of levee parallel to the river, the resulting floodplain area will generally increase because the boundary will be linearly interpolated from a cross-section upstream of the levee to the cross-section just downstream of any cross-section being removed. In reality, the floodplain boundary should follow the levee border, but because of the linear

interpolation process between cross-sections, the HEC-GeoRAS boundary is not the same as the levee boundary. If a cross-section is removed upstream/downstream of the upstream/downstream perpendicular section of the levee, the floodplain area will either increase or decrease depending on the width of inundation along the cross-section just upstream/downstream of any cross-sections removed. Figure 5.8 and Figure 5.9 present a section of the floodplain located near a levee with four cross-sectional modifications for the integrated DEM and NED 30 m DEM, respectively.

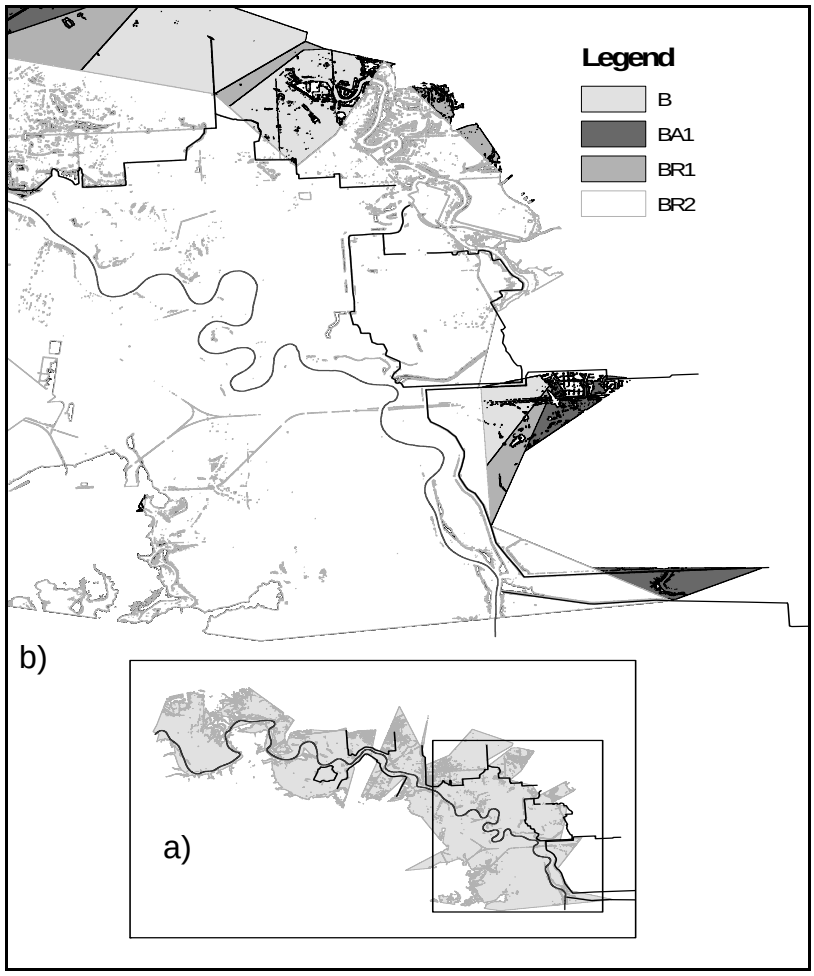

Figure 5.8 Inundation Boundary for the NED 30 m DEM for a) Entire Reach; b) Magnified Section for Four Cross-Sectional Modifications

For the integrated DEM, changing the cross-sectional configuration near levees is shown to cause large changes in the floodplain. For modification BA1, a cross-section is added just upstream of the perpendicular section of the levee causing an increase in the inundation area. For modifications BR1, cross-sections are removed from the section of levee running parallel to the river causing an increase in inundation area at this section. For modification BR2, cross-sections are removed both upstream of the perpendicular section of the levee and along the parallel section of the levee causing the floodplain area to be substantially reduced at this location.

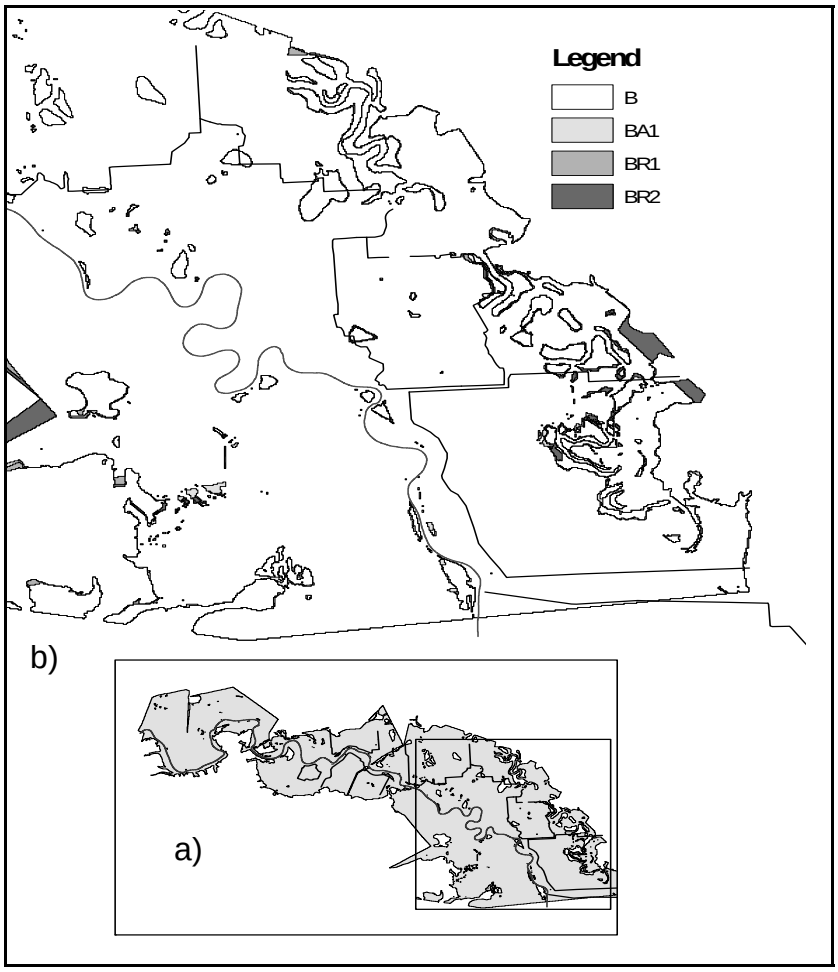

Figure 5.9 Inundation Boundary for the NED 30 m DEM for a) Entire Reach; b) Magnified Section for Four Cross-Sectional Modifications

For the lower resolution DEMs, changing the cross-sectional configuration in the vicinity of the levees causes little change because each cross-sectional modification shows levee overtopping. Changing the cross-sectional modification for the lower resolution DEMs generally results in a decrease in the inundation extent.

Table 5.6 presents the average width of inundation for each of the four DEMs for each cross-sectional modification. For the integrated DEM, inundation extent is complex near levee locations, and may cause an increase or decrease in the average width of inundation depending on the configuration of the cross-section locations. For the lower resolution DEMs, when cross-sections are added on bends in the river, the inundation extent increases, and when cross-sections are removed from bends in the river, inundation extent decreases. For cross-sections located on straight reaches of the river, removing a cross-section generally results in a decrease in inundation length along that cross-section.

Table 5.6 Average Width of Inundation (mi)

	NED 30 m	NED 10 m	LiDAR	Integrated
B	4.23	4.22	4.23	3.82
BA1	4.19	4.21	4.20	3.76
BA2	4.26	4.24	4.13	3.62
BA3	4.23	4.21	4.23	3.79
BR1	4.14	4.13	4.18	3.69
BR2	4.04	4.05	4.15	3.67
BR3	4.23	4.21	4.23	3.81
BR4	4.22	4.21	4.21	3.80
BR5	4.20	4.21	4.22	3.78
BR6	4.25	4.23	4.18	3.83
BR7	4.22	4.21	4.22	3.81
BR8	4.23	4.20	4.25	3.84

By removing one or a series of cross-sections from the higher resolution DEMS, the maximum increase in inundation width is 25 % while the maximum decrease is 22%. For the lower resolution DEMs, a maximum change in average width of inundation is 7 % when one or a series of cross-sections are removed. Similar to the results from Strouds

Creek, cross-sectional modifications alter the floodplain more for higher resolution DEMs.

5.4. Effect of Topography on the two-dimensional hydraulic model

In this section, four DEMs are evaluated for hydraulic modeling and floodplain mapping using the 10 foot mesh resolution for Strouds Creek and the 125 foot mesh resolution for the Brazos River. The extent of inundation is measured by the area of inundation and the average width of inundation along the cross-sections.

5.4.1. Strouds Creek

Table 5.7 presents the area of inundation as well as the average width of inundation and the percent change in inundation area using the integrated DEM as the benchmark for each of the four DEMs being evaluated for the 10 foot mesh resolution.

Table 5.7 Inundation for the 10 ft mesh resolution

	NED 30 m	NED 10 m	LiDAR	Integrated
Area (mi^2) (% change)	0.153 (17.44)	0.150 (15.70)	0.143 (10.53)	0.130 (0.00)
Average Width (ft)	274.97	268.23	250.78	224.13

Table 5.7 shows that increasing the DEM resolution produces the least inundation area. The integrated DEM produces the least extent of inundation area, followed by the LiDAR, NED 10m, and NED 30m DEMs. The area of inundation for the NED 30 m DEM is approximately 17% larger than that of the integrated DEM. The results for average width of inundation in Table 5.7 also show increasing inundation as the resolution of the DEM decreases. The average width of inundation increases from 224 to 275 feet from the integrated to the NED 30 m DEM. Figure 5.10 presents the floodplain for a section of Strouds Creek developed using FESWMS at a 10 foot mesh resolution for each DEM.

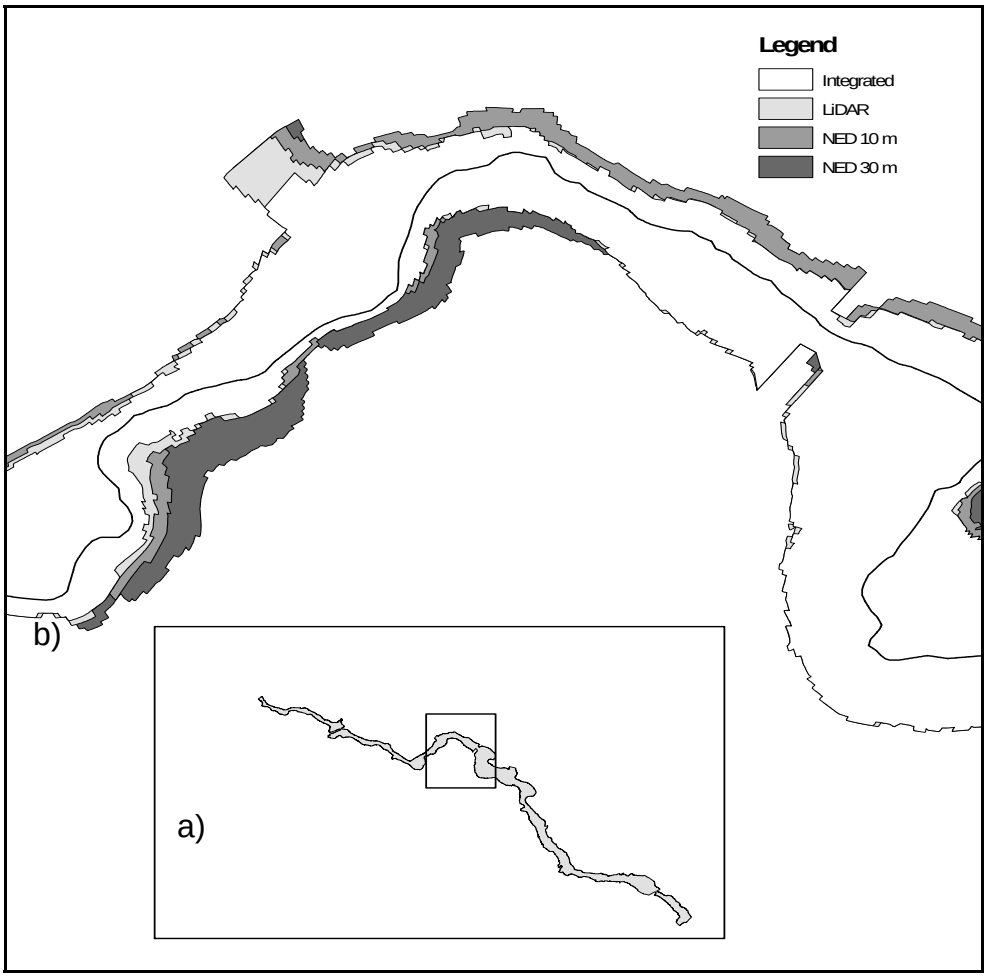

Figure 5.10 Inundation Boundary for a) Entire Reach; b) Magnified to a Bend in the River for the FESWMS 10 foot mesh resolution.

For each floodplain boundary shown in Figure 5.10, there is a slight increase in inundation area as the resolution of the DEM is decreased. There is also a shift in the representation of the floodplain between the higher and lower resolution DEMs. This figure shows the boundary of the integrated and LiDAR DEMs to be nearly identical, while there is a slight shift in the floodplain boundary for the NED 10 m DEM and a clear shift in the floodplain boundary for the NED 30 m DEM.

5.4.2. Brazos River

The results of effect of topographic representation for the two-dimensional model are shown in Table 5.8 for the 125 foot mesh resolution.

Table 5.8 Inundation for the 125 ft mesh resolution

	NED 30 m	NED 10 m	LiDAR	Integrated
Area (mi^2) (% change)	16.84 (7.62)	16.57 (5.95)	16.64 (6.35)	15.64 (0.00)
Average Width (mi)	3.24	3.24	3.28	2.98

Similar to the results from Strouds Creek, as the resolution of the DEM decreases, the inundation area increases. The maximum increase in inundation area for the Brazos River is below 8 %, while maximum increase in inundation area for Strouds Creek is above 17%. The Brazos River is affected less by changes in DEM because the representation of the main channel becomes less important for higher flows. Both the average width and inundation area are similar for the NED 30 m, NED 10 m, and LiDAR DEMs. Figure 5.11 presents the floodplain for a section of the Brazos River developed using FESWMS at a 125 foot main channel mesh resolution mesh resolution for each of the four DEMs being considered.

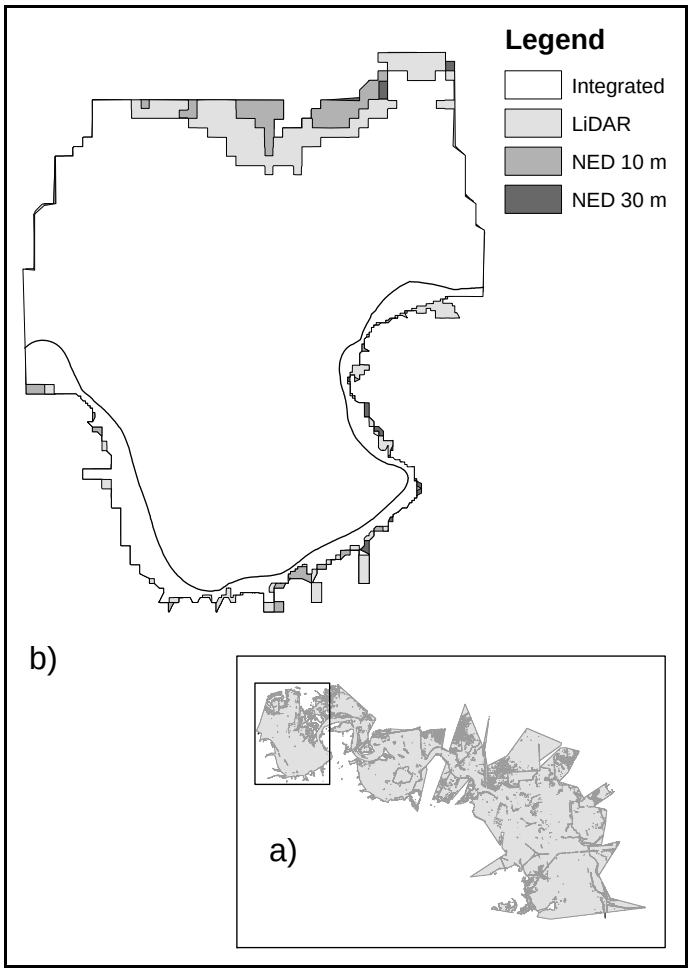

Figure 5.11 Inundation Boundary for 125 ft Mesh Resolution for a) Entire Reach; b) Upstream Section

Figure 5.11 shows the upstream, 9 mile reach of the Brazos River for four different DEMs. The images show that the inundation extent is similar for each of the four DEMs being considered, although the integrated DEM boundary shows slightly less inundation on the northern side of the river. For each of the four DEMs being analyzed, the flow does not extend to the floodplain on the southern side of the river because the main channel is steep and extends to a higher elevation on that side. Figure 5.12 shows cross-section station 206697.9 feet for the integrated DEM. This figure shows the large bank on the southern side of the Brazos River preventing flow into this floodplain on the nine mile upstream section being modeled in FESWMS.

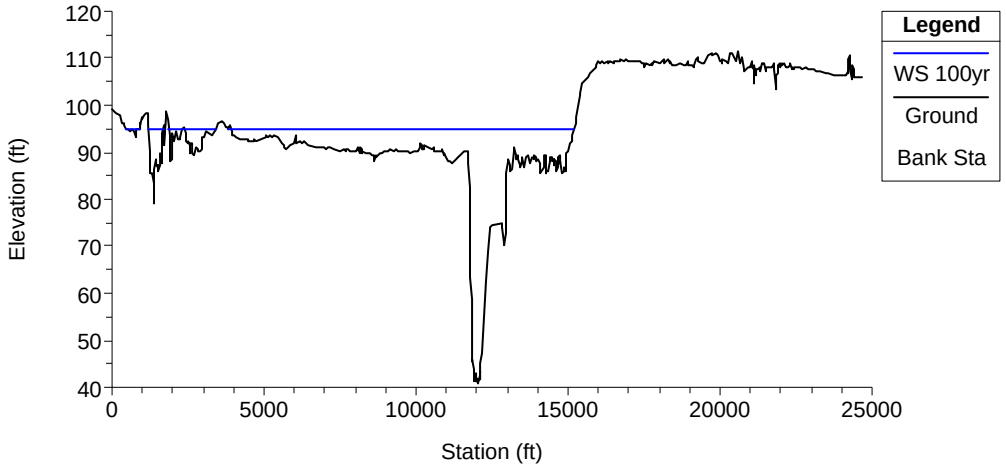

Figure 5.12 Cross-section showing large bank on south side of the Brazos River

5.5. Effect of Geometry on two-dimensional hydraulic model

In this section, four DEMs are evaluated for hydraulic modeling and floodplain mapping using 2 mesh resolutions for Strouds Creek and 2 mesh resolutions for the Brazos River. The extent of inundation is measured by the area of inundation and the average width of inundation along the original cross-sections.

5.5.1. Strouds Creek

Table 5.9 presents the area of inundation as well as the percent change in inundation area using the 10 foot mesh resolution as the benchmark for four DEMs and for two mesh resolutions.

Table 5.9 Inundation Area (mi^2) (% Change)

	NED 30 m	NED 10 m	LiDAR	Integrated
10-ft Mesh Resolution	0.153 (0.00)	0.150 (0.00)	0.143 (0.00)	0.130 (0.00)
20-ft Mesh Resolution	0.151 (-1.00)	0.144 (-3.92)	0.137 (-4.22)	0.127 (-2.58)

The results of Table 5.9 show that the 20 foot mesh resolution produces a smaller area of inundation for each of the four DEMs, although the maximum decrease in inundation area from the 10 foot to the 20 foot mesh resolution is below 5 %. To further show how mesh resolution changes the extent of inundation, Table 5.10 presents the average width of inundation for each of the four DEMs for two mesh resolutions.

Table 5.10 Average Width of Inundation (ft)

	NED 30 m	NED 10 m	LiDAR	Integrated
10-ft Mesh Resolution	274.97	268.23	250.78	224.13
20-ft Mesh Resolution	269.88	256.19	239.48	221.00

Similar to the results of Table 5.9, the results of this table suggest that the 10 foot mesh resolution produces a larger inundation extent than that of the 20 foot mesh resolution for Strouds Creek, although the change in average width never exceeds 5 %.

5.5.2. Brazos River

The results for the effect of mesh resolution on the inundation extent are presented in

Table 5.11 The percent change is in reference to the 125 foot mesh resolution.

Table 5.11 Inundation Area (mi^2) (% Change)

	NED 30 m	NED 10 m	LiDAR	Integrated
FESWMS 125-ft Resolution	16.84 (0.00)	16.57 (0.00)	16.64 (0.00)	15.64 (0.00)
FESWMS 250-ft Resolution	16.81 (-0.16)	16.94 (2.21)	17.02 (2.30)	15.85 (1.29)

Contrary to the results for Strouds Creek where the higher resolution mesh produces the larger inundation area, the lower resolution mesh produces a larger inundation area for three of the four DEMs. Similar to the results from Strouds Creek, the change in inundated area from one mesh resolution to another is small and never exceeds 2.5 %.

The only DEM to predict more inundation area for the 250 foot main channel mesh resolution is the NED 30 m DEM. Table 5.12 provides further information as to the extent of inundation for differing mesh resolutions. The average width of inundation for each DEM is very similar between the 125 foot and 250 foot main channel mesh resolutions. The largest change is seen in the LiDAR DEM where the average width increases by over 6 % from the 125 to the 250 foot main channel mesh resolution.

Table 5.12 Average Width of Inundation (mi)

	NED 30 m	NED 10 m	LiDAR	Integrated
FESWMS 125-ft Resolution	3.24	3.24	3.28	2.98
FESWMS 250-ft Resolution	3.19	3.28	3.49	3.05

5.6. Comparison of HEC-RAS and FESWMS

In this section, the one-dimensional model HEC-RAS and the two-dimensional model FESWMS are compared for hydraulic modeling and flood inundation mapping. For both FESWMS and HEC-RAS, changes in topography and geometry are considered. The extent of inundation is measured by the area of inundation and the average width of inundation along the original cross-sections.

5.6.1. Strouds Creek

Table 5.13 presents the inundation area for each of the HEC-RAS cross-sectional modification (except those where only one or a series of cross-sections were removed) and for both FESWMS mesh resolutions for each of the four DEMs. To compare the results of the HEC-RAS simulations with those of the FESWMS simulations, all HEC-RAS inundation boundary polygons are clipped to the same length as those developed using FESWMS.

Table 5.13 Inundation Area (mi^2)

	Area of Inundation (mi^2)			
	NED 30 m	NED 10 m	LiDAR	Integrated
S	0.171	0.155	0.128	0.109
SA1	0.173	0.156	0.134	0.115
SA2	0.174	0.156	0.138	0.119
SA3	0.173	0.156	0.137	0.117
SR1	0.171	0.153	0.116	0.100
SR2	0.168	0.152	0.107	0.091
SI1	0.175	0.157	0.136	0.118
SI2	0.171	0.156	0.130	0.111
SI3	0.170	0.157	0.123	0.103
10-ft	0.153	0.150	0.143	0.130
20-ft	0.151	0.144	0.137	0.127

From Table 5.13, it is seen that the inundated area for the HEC-RAS analysis is larger than the inundated area for the FESWMS analysis for the lower resolution DEMs and smaller than the inundated area for the FESWMS analysis for the higher resolution DEMs. These results also suggest that HEC-RAS is more susceptible to a change in DEM than FESWMS as the increase in area from the high resolution DEMs to the high resolution DEMs is larger for HEC-RAS. For the HEC-RAS simulations, the area increases by around 0.6 mi^2 for some cross-sectional modifications while the area increases by approximately 0.2 mi^2 for the FESWMS simulations.

The results of Table 5.13 also show that the LiDAR and NED 10 m DEMs most closely predict the inundation area between HEC-RAS and FESWMS while the integrated and NED 30 m DEMs produce inundation area results very different between HEC-RAS and FESWMS. Figure 5.13 shows the floodplain developed from the FESWMS 10 foot mesh resolution along with the floodplain developed using four HEC-RAS cross-sectional configurations for the integrated DEM. In this figure, the floodplain produced in HEC-RAS for the original cross-sections shows discontinuities in the floodplain which are not seen in the FESWMS floodplain. The SA1 modification shows a floodplain more similar to the FESWMS simulation. The SR1 and SR2 modifications show results very different than the results of the FESWMS simulation as the floodplain becomes degraded when

cross-sections are removed. This figure as well as the results of Table 5.13 suggest that, for the higher resolution DEMs, the results from the HEC-RAS simulations become more similar to the results of the FESWMS simulations when cross-sections are added. Although increasing the number of HEC-RAS cross-sections produces an area more similar to FESWMS simulation results, each HEC-RAS simulation resulted in an area less than any FESWMS simulation for the integrated DEM.

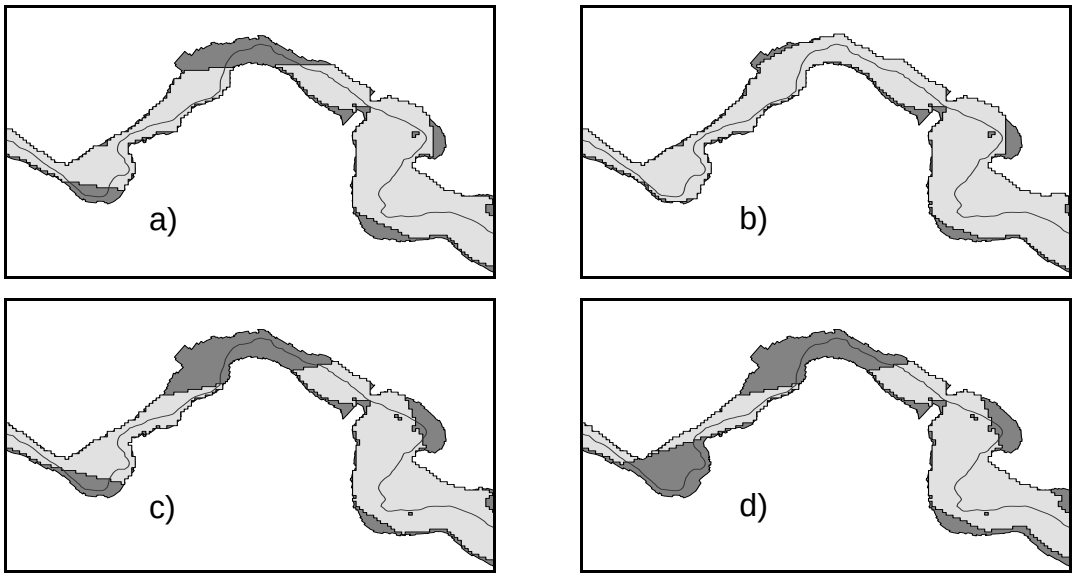

Figure 5.13 Inundation Boundary for 10 ft Mesh Resolution and a) S; b) SA1; c) SR1; d) SR2 for the Integrated DEM

Figure 5.14 shows the floodplain developed from the FESWMS 10 foot mesh resolution along with the floodplain developed using four HEC-RAS cross-sectional configurations for the NED 30 m DEM. Because the original HEC-RAS cross-sectional modification overestimated the FESWMS simulated area, reducing the number of HEC-RAS cross-sections produces an area more similar to that of the FESWMS simulations. It should be noted that although reducing the number of cross-sections in HEC-RAS produces an area more similar to that of the FESWMS simulations, each HEC-RAS simulation predicted an area larger than any FESWMS simulation for the lower resolution DEMs.

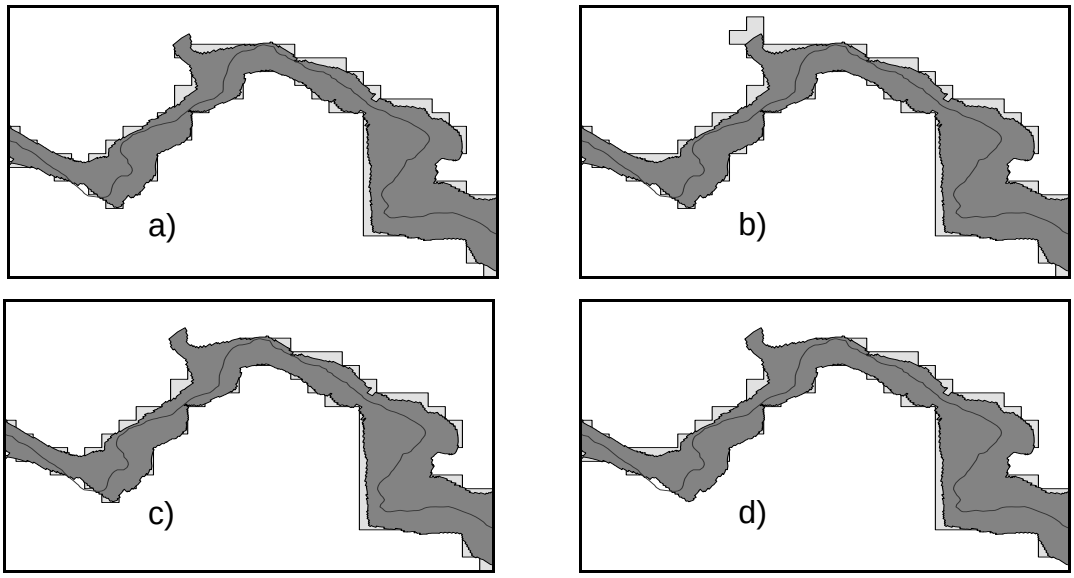

Figure 5.14 Inundation Boundary for 10 ft Mesh Resolution and a) S; b) SA1; c) SR1; d) SR2 for the NED 30 m DEM

To further show that the HEC-RAS simulations for the high resolution DEMs predict larger inundation extents than those of FESWMS and for the lower resolution predict smaller inundation extents than those of FESWMS, Table 5.14 presents the average width of inundation along the original cross-sections for each FESWMS and HEC-RAS simulation. Conclusions from this table coincide with those presented in Table 5.13.

Table 5.14 Average Width of Inundation (ft)

	NED 30 m	NED 10 m	LiDAR	Integrated
S	311.57	281.30	249.13	203.33
SA1	310.71	278.90	249.56	202.62
SA2	309.25	280.30	251.04	207.98
SA3	314.21	280.04	248.78	203.72
SR1	313.86	282.41	229.22	189.15
SR2	305.50	285.58	215.97	174.23
SI1	311.86	280.68	255.15	211.71
SI2	310.66	280.40	247.81	206.78
SI3	304.05	282.67	241.22	196.89
10-ft	274.97	268.23	250.78	224.13
20-ft	269.88	256.19	239.48	221.00

5.6.2. Brazos River

The results comparing the inundation area from the HEC-RAS analysis with the FESWMS analysis for the Brazos River are presented in Table 5.15.

Table 5.15 Inundation Area (mi^2)

	Area of Inundation (mi^2)			
	NED 30 m	NED 10 m	LiDAR	Integrated
B	16.43	16.43	16.42	13.00
BA1	16.13	15.93	16.46	13.69
BA2	16.00	15.84	16.39	13.44
BA3	16.16	16.17	16.43	13.48
BR1	16.29	16.20	16.53	12.27
BR2	12.73	12.66	12.90	10.57
125-ft	16.84	16.57	16.64	15.64
150-ft	16.81	16.94	17.02	15.85

The results of Table 5.15 show that the inundated area from FESWMS is always larger than that of HEC-RAS. For the integrated DEM, the inundated area produced in FESWMS is substantially larger than the inundated area produced in HEC-RAS. For the other three DEMs being analyzed, the inundated areas produced from FESWMS and HEC-RAS are more similar. For the NED 10 m and LiDAR DEMs, the FESWMS 125 foot mesh resolution and most HEC-RAS cross-sectional modifications produce similar results. The FESWMS simulations for the NED 30m DEM predict an area larger than any area predicted using a HEC-RAS simulation.

Similar to the results from Strouds Creek, Table 5.15 shows that HEC-RAS is more susceptible to changes in DEM than is FESWMS. The difference in inundated area from the FESWMS simulation for the integrated DEM to the lower resolution DEMs is less than 1.2 mi^2. For the HEC-RAS analysis, the difference in inundated area between the integrated DEM and the lower resolution DEMs is above 3 mi^2 for some of the cross-sectional modifications. This table also shows that by increasing the number of cross-sections (BA1, BA2, and BA3) for analysis of the integrated DEM the inundated area

becomes closer to the inundated area predicted by FESWMS. For the two lower resolution DEMs and the LiDAR DEM, all cross-sectional modifications produce similar floodplain areas to the FEWSMS floodplain area with the exception of the one-third cross-sectional modification. The one-third cross-sectional modification produces an area much less than any other modification due to much of the area being cut off when the floodplain boundary is interpolated between cross-sections.

Figure 5.15 and Figure 5.16 present the inundation boundaries for the FESWMS 125 foot main channel mesh resolutions and four HEC-RAS cross-sectional modifications for the integrated and NED 30 m DEMs, respectively.

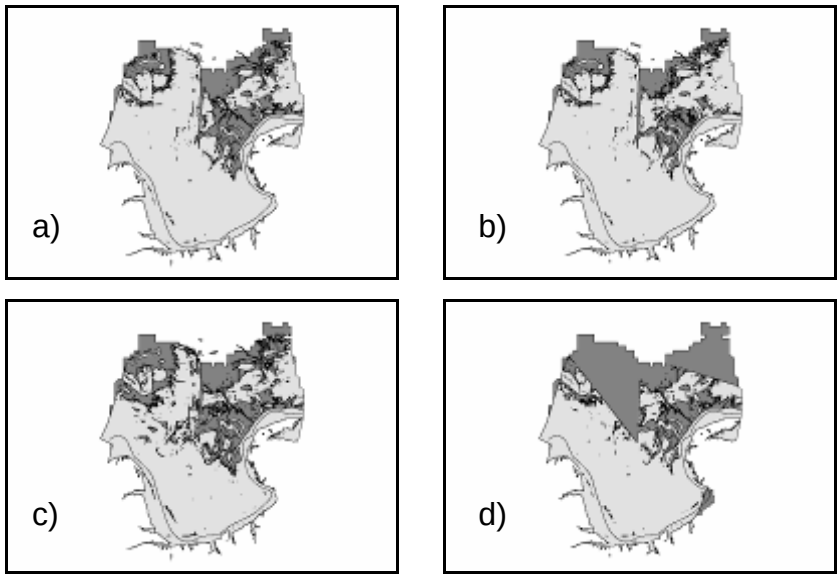

Figure 5.15 Inundation Boundary for 125 ft Mesh Resolution and a) S; b) SA1; c) SR1; d) SR2 for the Integrated DEM

Similar to what is seen for Strouds Creek, increasing the number of HEC-RAS cross-sections when using the integrated DEM produces an area more similar to that of FESWMS, although FESWMS produces a continuous floodplain while HEC-RAS produces discontinuous floodplain. This is due to the process by which HEC-GeoRAS

subtracts the topographic data from the water surface elevations to determine the floodplain.

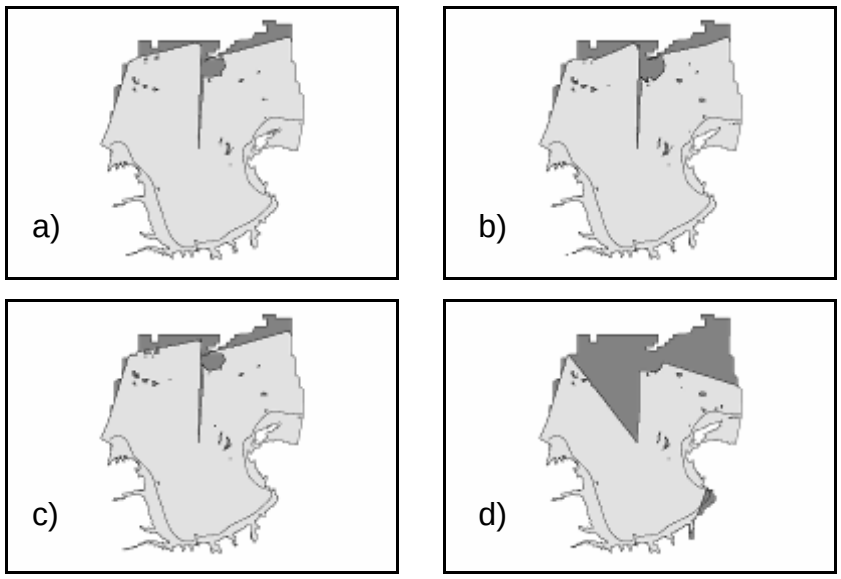

Figure 5.16 Inundation Boundary for 125 ft Mesh Resolution and a) S; b) SA1; c) SR1; d) SR2 for the NED 30 m DEM

Figure 5.16 shows that the floodplain extent for the original cross-sectional configuration and modifications BA1 and BR1 are similar and that the floodplain boundary from the FESWMS simulation is greater than any HEC-RAS boundary. Contrary to what is seen in the results for Strouds Creek, the BR2 modification causes a large change in inundation extent for the lower resolution DEMs.

CHAPTER 6. SUMMARY AND CONCLUSIONS

6.1. Effect of topography on 1D and 2D hydraulic models

The first objective of this research is to evaluate the effect of topography on both a one- and a two-dimensional hydrodynamic model. This is accomplished by using four DEMs; integrated, LiDAR, NED 10m, and NED 30 m to produce floodplain maps using HEC-RAS and FESWMS for Strouds Creek in North Carolina and the Brazos River in Texas. For both river reaches evaluated, both the area of inundation and average width of inundation along the original cross-sections increase as the resolution of the DEM decreases. For Strouds Creek, the NED 30 m DEM produces an area 65 % larger than that of the integrated DEM, while for the Brazos River, the NED 30 m DEM produces an area approximately 26 % larger than that of the integrated DEM using HEC-RAS. The average width of inundation increases by over 60 % for Strouds Creek and by approximately 11 % for the Brazos River from the integrated DEM to the NED 30 m DEM.

From the two-dimensional floodplain mapping process, the inundation area for Strouds Creek for the NED 30 m DEM is 17 % larger than the inundation area for the integrated DEM, and for the Brazos River, the inundation area for the NED 30 m DEM is 8 % larger than that of the integrated DEM. The average width of inundation increases by nearly 23 % for Strouds Creek and by nearly 9 % for the Brazos River from the integrated DEM to the NED 30 m DEM.

The reason for a larger change between the low and high resolution DEMs for Strouds Creek is that the 100-year flow is a relatively small value causing most of the water to be routed through the main channel. When most of the flow is routed through the main

channel, the main channel topographic representation becomes very important. For the Brazos River, with a high flow rate, most of the flow is routed through the floodplains making the topographic representation of the main channel less important.

Results from this thesis are similar to those found in other studies that decreasing resolution of the topographic data causes an increase in the floodplain area. In studies performed by Sanders (2007) and Casas et al. (2007) it was found that increasing the resolution of the DEM leads to a decrease in inundated area.

6.2. Effect of geometry on 1D and 2D hydraulic models

The second topic addressed in this thesis is the effect of geometry on one- and two-dimensional hydraulic models. For the one-dimensional HEC-RAS model, 18 cross-sectional configurations are analyzed for Strouds Creek and 12 cross-sectional configurations are analyzed for the Brazos River. For Strouds Creek, increasing the number of cross-sections generally results in an increase in the inundation extent. For the Brazos River, the same trend is seen that increasing the number of cross-sections increases the inundation extent for the higher resolution DEMs except in the vicinity of the levees. Changing the cross-sectional configuration near levees produces complex results and produces significant changes in both inundation area and width of inundation along the cross-sections. Removing specific cross-sections generally results in a decrease in width of inundation along the cross-section removed for both river reaches analyzed except when the cross-section being removed is located near a levee. Cross-sections sufficiently far up or downstream are unaffected by a single or consecutive cross-sections being removed. Cross-section modifications are shown to alter results for higher resolution DEMs more than for lower resolution DEMs. Similar to the results found in a study by Samuels (1990), cross-sectional configuration is important in hydraulic modeling and floodplain mapping.

For the two-dimensional FESWMS model, two mesh resolutions are tested for both Strouds Creek and the Brazos River. For Strouds Creek, the 10 foot mesh resolution produces a larger inundation area than the 20 foot mesh resolution for each of the four DEMs being analyzed. The maximum change in inundation area between the two mesh resolutions for Strouds Creek is less than 5 %. For the Brazos River, the 250 foot mesh resolution is shown to produce a larger inundation area than the 125 foot mesh resolution for three of the four DEMs analyzed, although by a maximum value of only 2.3 %. In a study performed by Hardy et al. (1998), it was found that increasing the mesh resolution results in a decrease in inundation area similar to what was found in this thesis for the Brazos River. A study by Horritt et al. (2006) suggests that two-dimensional models are sensitive to changes in mesh resolution.

6.3. Comparison of 1D and 2D Hydraulic Models

The final objective of this thesis is to compare the results from HEC-RAS and FESWMS in flood inundation mapping. The 18 cross-sectional configurations for Strouds Creek and 12 cross-sectional configurations for the Brazos River are compared to the two mesh resolutions for each river reach using four DEMs. It is found that the HEC-RAS model is more susceptible to changes in DEM than the FESWMS model. For Strouds Creek, the percent change in inundation area from the integrated DEM to the NED 30 m DEM for the HEC-RAS simulations is approximately 57 % and for the FESWMS simulations is 18 %. For the Brazos River, the percent change in inundation area from the lower resolution DEMs to the high resolution DEMs is 26 % for the HEC-RAS simulations and 8 % for the FESWMS simulations.

For the higher resolution DEMs, LiDAR and integrated for Strouds Creek and integrated for the Brazos River, FESWMS predicts a larger area than HEC-RAS. For the lower resolutions DEMs for Strouds Creek, HEC-RAS predicts a larger inundation area, and the three remaining DEMs for the Brazos River predict approximately equal areas using both HEC-RAS and FESWMS. For the higher resolution DEMs, the HEC-RAS area becomes

more similar to that of FESWMS when cross-sections are added to the simulations. For Strouds Creek using the lower resolution DEMs, the results from HEC-RAS and FESWMS become more similar when cross-sections are removed. Changing mesh resolution or cross-sectional configuration is found to have less of an affect on the resulting floodplain than changes in the DEM. Results from this thesis are similar to that of other studies in which the results from one- and two-dimensional models are found to produce different floodplain areas (Juza and Barad, 2000, Schumann et al., 2007).

The one-dimensional HEC-RAS model linearly interpolates the floodplain boundary between cross-sections, and then defines the floodplain by subtracting the topographic data from the water surface elevations. This process often results in a discontinuous floodplain. The advantage of using the one-dimensional floodplain mapping process is that is easy to use and produces results quickly. In a HEC-RAS simulation, the Manning's n value is often used as the lone calibrating parameter, and can change results significantly (HEC, 2002). Where the HEC-RAS simulation takes a matter of seconds to complete, the FESWMS simulation can take multiple hours. The advantage of the two-dimensional model is that it produces a continuous floodplain as it represents the topography as a series of mesh elements and can model flow in both the lateral and longitudinal directions resulting in a more accurate representation of the floodplain. For a FESWMS simulation, two calibrating parameters, Manning's n and eddy viscosity, can be used as calibrating parameters and may have an affect of the results of the hydraulic simulations (FESWMS, 2002). The experience of the modeler can have an affect on the resulting floodplain due to the calibrating parameters in both the one- and two-dimensional model and the meshing type in the two-dimensional model.

6.4. Future Work

Future work on hydraulic modeling and flood inundation mapping using 1D and 2D models should consider the effect of the calibrating parameters, Manning's n for HEC-RAS and both Manning's n and eddy viscosity for FESWMS. These parameters should

be used to calibrate and validate the models to be used and compared against known historical high water marks or floodplain boundaries.

Future work should also consider a broader range of mesh resolutions in FESWMS as well as the effect of meshing type. Due to the lack of computing capabilities of the machine used to perform the FESWMS simulations, very high mesh resolutions could not be examined. As the computing capabilities are increased, the effect of the levees in FESWMS should also be examined for the Brazos River.

To further evaluate the effects of topographic data, geometric data, and type of model used on hydraulic modeling and flood inundation mapping, more study areas should be evaluated. These study areas should include a broad range of characteristics including length of the river reach, width of the floodplain, slope, bridges and levees, and land use. Other one- and two-dimensional models should also be used to compare results.

LIST OF REFERENCES

Bates, P.D., and De Roo, A.P.G. A Simple Raster-Based Model for Flood Inundation Simulation. Journal of Hydrology, 236.1-2 (2000): 54-77.

Bates P.D., Marks K.J., Horritt M.S. Optimal use of high-resolution topographic data in flood inundation models. Hydrological Processes 17 (2003): 537- 557.

Bates, P.D., Horritt, M.S., Hunter, N.M., Mason, D., Cobby, D. Numerical modelling of floodplain flow. Computational Fluid Dynamics: Applications in Environmental Hydraulics, 2005 John Wiley & Sons, Ltd. 271 – 297.

Brandt, S.A. Resolution issues of elevation data during inundation modeling of river floods. Proc. XXXI Int. Association of Hydraulic Engineering and Research Congress, Water Engineering for the Future: Choices and Challenges, September 11 – 16 (2005), Seoul, Korea: 3572 – 3581.

Casas A., Benito V.R., Thorndycraft V.R., Rico M. The topographic data source of digital terrain models as a key element in the accuracy of hydraulic flood modelling. Earth Surface Processes and Landforms 31 (2006): 444-456.

Charlton M.E., Large A.R.G., Fuller I.C. Application of airborne LiDAR in river environments: The River Coquet, Northumberland, UK. Earth Surface Processes and Landforms 28 (2003): 299-306.

Cobby D.M., Mason D.C., Davenport I.J. Image processing of airborne scanning laser altimetry for improved river flood modelling. ISPRS Journal of Photogrammetry and Remote Sensing 56 (2001): 121-138.

Crowder, D. W., and P. Diplas. Using Two-Dimensional Hydrodynamic Models at Scales of Ecological Importance. Journal of Hydrology, 230.3-4 (2000): 172-91.

Dutta, D., Alam, J., Umeda, K., Hayashi, M., Hironaka, S. A two-dimensional hydrodynamic model for flood inundation simulation: a case study in the lower Mekong river basin. Hydrologic Processes 21 (9) (2007): 1223 – 1237.

FESWMS FST2DH User's Manual. Federal Highway Administration. Publication number FHWA-RD-03-053 (2002).

Haile, A.T. and Rientjes T.H.M., Effects of LiDAR DEM resolution in flood modelling: a model sensitivity study for the city of Tegucigalpa, Honduras. International Archives of Photogrammetry, Remote Sensing and Spatial Information Sciences 36 (Part 3/W19) (2005): 168–173.

Hardy, R.J., Bates, P.D. and Anderson, M.G. The Importance of Spatial Resolution in Hydraulic Models for Floodplain Environments. Journal of Hydrology, 216.1-2 (1999): 124-36.

HEC-GeoRAS user's manual available at www.hec.usace.army.mil/software/hec-ras/hec-georas.html.

HEC-RAS hydraulic reference manual available at www.hec.usace.army.mil/ software/hec-ras/hec-georas.html.

HEC-RAS user's manual available at www.hec.usace.army.mil/software/hec-ras/.

Hodgson, M.E., Jensen, J.R., Schmidt, L., Schill, S., Davis, B. An Evaluation of LIDAR- and IFSAR-Derived Digital Elevation Models in Leaf-on Conditions with USGS Level 1 and Level 2 DEMs. Remote Sensing of Environment, 84.2 (2003): 295-308.

Horritt, M. S., and Bates, P.D. Effects of Spatial Resolution on a Raster Based Model of Flood Flow. Journal of Hydrology, 253.1-4 (2001): 239-49.

Horritt, M.S., and Bates, P.D. Evaluation of 1D and 2D Numerical Models for Predicting River Flood Inundation. Journal of Hydrology, 268.1-4 (2002): 87-99.

Horritt, M.S., P.D. Bates, and M.J. Mattinson. Effects of Mesh Resolution and Topographic Representation in 2D Finite Volume Models of Shallow Water Fluvial Flow. Journal of Hydrology, 329.1-2 (2006): 306-14.

Hunter, N.M., Bates, P.D., Horritt, M.S., Wilson, M.D. Simple Spatially-Distributed Models for Predicting Flood Inundation: A Review. Geomorphology, 90.3-4 (2007): 208-225.

Juza, B., and Barad, M. Dynamic and steady state modeling approaches to riverine hydraulic studies using 1-D, looped 1-D and 2-Dimensional topological discretization. www.engr.ucdavis.edu/~edllab/Users/Barad/Papers/Hydroinformatics2000.pdf.

Kelly, B.P., Rydlund Jr., P.H. Estimated Flood-Inundation Mapping for the Lower Blue River in Kansas City, Missouri. USGS Scientific Investigations Report 2006-5089 (2003-2005).

Leopardi A, Oliveri E, Greco M. Two-dimensional modeling of floods to map risk-prone area. Journal of Water Resources Planning and Management (2002): 168-178.

Mason DC, Cobby DM, Horritt MS, Bates PD. Floodplain friction parameterization in two-dimensional river flood models using vegetation heights derived from airborne scanning laser altimetry. Hydrological Processes 17 (2003): 1711-1732.

McMillan, Hilary K., and James Brasington. Reduced Complexity Strategies for Modelling Urban Floodplain Inundation. Geomorphology, 90.3-4 (2007): 226-243.

Merwade, V. Tutorial on using HEC-GeoRAS with ArcGIS 9.1. (2006). http://web.ics.purdue.edu/~vmerwade/education/georastutorial.pdf

Merwade, V., Cook, A., Coonrad, J. GIS techniques for creating river terrain models for hydrodynamic modeling and flood inundation mapping. A possible submission to Environmental Modelling and Software (2007).

Mohammed, T.A., Said, S., Bardaie, M.Z., Basri, S. One-Dimensional Simulation of Flood Levels in a Tropical River System Using HEC-2 Model. Joint International Conference on Computing and Decision Making in Civil and Building Engineering, June 14 – 16 (2006): Montreal, Canada.

Musser, J.W., Dyar T.R. Two-Dimensional Flood-Inundation Model of the Flint River at Albany, Georgia. Proceedings of the 2005 Georgia Water Resources Conference, April 25 – 27 (2005): University of Georgia, Athens, Georgia.

Noman, N.S., Nelson, E.J., Zundel, A.K. Review of automated flood plain delineation from digital terrain models. Journal of Water Resource Planning and Management, 127 (2001): 394-402.

O'Brien, J. S., Julien, P. Y. and Fullerton, W. T. Two-dimensional water flood and mudflow simulation. Journal of the Hydraulics Division, ASCE, 119 (1993): 244-261.

Omer C.R., Nelson E.J., Zundel A.K. Impact of varied data resolution on Hydraulic Modeling and Floodplain Delineation. Journal of the American Water Resources Association 39 (2) (2003): 467- 475.

Papanicolaou, A., Elhakeem, M. Hydraulic performance of shallow water habitat in the Missouri River for ecological studies.. Proceedings of the 7th International Conference on HydroScience and Engineering September 10- 13 (2006): Philadelphia, USA.

Samuels, P.G. Cross-section location in 1-D models. International Conference on River Flood Hydraulics, September 17 – 20 (1990).

Sanders, Brett F. Evaluation of on-Line DEMs for Flood Inundation Modeling. Advances in Water Resources, 30.8 (2007): 1831-43.

Schumann, G., Matgen, P., Cutler, M.E.J., Black, A., Hoffman, L., Pfister, L. Comparison of Remotely Sensed Water Stages from LiDAR, Topographic Contours and SRTM. ISPRS Journal of Photogrammetry and Remote Sensing, In Press, Corrected Proof.

Sinnakaudan S, Ab Ghani A, Chang C.K. Flood inundation analysis using HEC-6 and ArcView GIS 3.2a. In Proceeding, 5th International Conference on Hydro-Science & Engineering, September 18–21 (2002), Warsaw University of Technology, Poland.

Smith MJ, Edwards EP, Priestnall G, Bates PD. Exploitation of new data types to create digital surface models for flood inundation modeling, FRMRC Research Report UR3, FRMRC, UK: (2006). www.floodrisk.org.uk.

SMS version 9.2 tutorials. Brigham Young University, Environmental Modeling Research Laboratory (2006).

Tayefi, V., Lane, S.N., Hardy, R.J., Yu, D. A comparison of one- and two-dimensional approaches to modeling flood inundation over complex upland floodplains. Hydrologic Processes 21 (2007): 3190 – 3202.

Wagner, C.R., Mueller, D.S., USGS. Calibration and Validation of a Two-Dimensional Hydrodynamic Model of the Ohio River, Jefferson County, Kentucky. Water Resources Investigations Report 01-4091 (2001).

Werner M, Blazkova S, Petr J. Spatially distributed observations in constraining inundation modelling uncertainties. Hydrological Processes 19 (2005): 3081-3096.

Wilson, M.D., Atkinson, P.M., A comparison of remotely sensed elevation datasets for flood inundation modeling. Proceedings of the 7th International Conference on Geocomputation (2003): University of Southampton, U.K.

Winters, K.E. Simulations of flooding Tchoutacabouffa River at State Highways 15 and 67 at D'lberville, Mississippi.. Water Resources Investigations Report 01-4007 (2000).

Zanichelli, G., Caroni, E., Fiorotto, V. River Bifurcation Analysis by Physical and Numerical Modeling. Journal of Hydraulic Engineering 130 – 3 (2004): 237-242.